Dalton Transactions c9dt04338a

We have presented the Graphical Abstract text and image for your article below. This brief summary of your work will appear in the contents pages of the issue in which your article appears.

1

Bis(alkyl) scandium and yttrium complexes coordinated by an amidopyridinate ligand: synthesis, characterization and catalytic performance in isoprene polymerization, hydroelementation and carbon dioxide hydrosilylation

G. A. Gurina, A. A. Kissel, D. M. Lyubov, L. Luconi, A. Rossin, G. Tuci, A. V. Cherkasov, K. A. Lyssenko, A. S. Shavyrin, A. M. Ob'edkov, G. Giambastiani* and A. A. Trifonov*

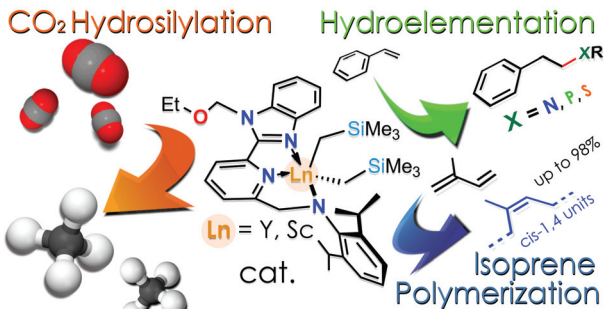

Highly versatile and robust organolanthanides as catalysts or catalyst precursors for a variety of challenging transformations.

Please check this proof carefully. Our staff will not read it in detail after you have returned it.

Please send your corrections either as a copy of the proof PDF with electronic notes attached or as a list of corrections. **Do not edit the text within the PDF or send a revised manuscript** as we will not be able to apply your corrections. Corrections at this stage should be minor and not involve extensive changes.

Proof corrections must be returned as a single set of corrections, approved by all co-authors. No further corrections can be made after you have submitted your proof corrections as we will publish your article online as soon as possible after they are received.

Please ensure that:

- The spelling and format of all author names and affiliations are checked carefully. You can check how we have identified the authors' first and last names in the researcher information table on the next page. **Names will be indexed and cited as shown on the proof, so these must be correct.**
- Any funding bodies have been acknowledged appropriately and included both in the paper and in the funder information table on the next page.
- All of the editor's queries are answered.
- Any necessary attachments, such as updated images or ESI files, are provided.

Translation errors can occur during conversion to typesetting systems so you need to read the whole proof. In particular please check tables, equations, numerical data, figures and graphics, and references carefully.

Please return your **final** corrections, where possible within **48 hours** of receipt, by e-mail to: dalton@rsc.org. If you require more time, please notify us by email.

Funding information

Providing accurate funding information will enable us to help you comply with your funders' reporting mandates. Clear acknowledgement of funder support is an important consideration in funding evaluation and can increase your chances of securing funding in the future.

We work closely with Crossref to make your research discoverable through the Funding Data search tool (http://search.crossref.org/funding). Funding Data provides a reliable way to track the impact of the work that funders support. Accurate funder information will also help us (i) identify articles that are mandated to be deposited in **PubMed Central (PMC)** and deposit these on your behalf, and (ii) identify articles funded as part of the **CHORUS** initiative and display the Accepted Manuscript on our web site after an embargo period of 12 months.

Further information can be found on our webpage (http://rsc.li/funding-info).

What we do with funding information

We have combined the information you gave us on submission with the information in your acknowledgements. This will help ensure the funding information is as complete as possible and matches funders listed in the Crossref Funder Registry.

If a funding organisation you included in your acknowledgements or on submission of your article is not currently listed in the registry it will not appear in the table on this page. We can only deposit data if funders are already listed in the Crossref Funder Registry, but we will pass all funding information on to Crossref so that additional funders can be included in future.

Please check your funding information

The table below contains the information we will share with Crossref so that your article can be found *via* the Funding Data search tool. **Please check that the funder names and grant numbers in the table are correct and indicate if any changes are necessary to the Acknowledgements text.**

Funder name	Funder's main country of origin	Funder ID (for RSC use only)	Award/grant number
Russian Academy of Sciences	Russia	501100002674	17-73-20262
Ministero dell'Istruzione, dell'Università e della Ricerca	Italy	501100003407	20179337R7
Agence Nationale de la Recherche	France	501100001665	ANR-17-MPGA-0017

Q1

Researcher information

Please check that the researcher information in the table below is correct, including the spelling and formatting of all author names, and that the authors' first, middle and last names have been correctly identified. **Names will be indexed and cited as shown on the proof, so these must be correct.**

If any authors have ORCID or ResearcherID details that are not listed below, please provide these with your proof corrections. Please ensure that the ORCID and ResearcherID details listed below have been assigned to the correct author. Authors should have their own unique ORCID iD and should not use another researcher's, as errors will delay publication.

Please also update your account on our online manuscript submission system to add your ORCID details, which will then be automatically included in all future submissions. See here for step-by-step instructions and more information on author identifiers.

First (given) and middle name(s)	Last (family) name(s)	ResearcherID	ORCID iD
G. A.	Gurina		0000-0002-2969-0856
A. A.	Kissel		
D. M.	Lyubov	A-6041-2016	0000-0001-8472-3764
L.	Luconi		0000-0003-4407-6026
A.	Rossin	P-6379-2015	0000-0002-1283-2803
G.	Tuci	T-5404-2017	0000-0002-3411-989X

A. V.	Cherkasov		0000-0001-8095-3562
K. A.	Lyssenko		
A. S.	Shavyrin		
A. M.	Ob'edkov		
G.	Giambastiani	E-3255-2016	0000-0002-0315-3286
A. A.	Trifonov	A-6065-2016	0000-0002-9072-4517

Queries for the attention of the authors

Journal: **Dalton Transactions** Paper: **c9dt04338a**

Title: **Bis(alkyl) scandium and yttrium complexes coordinated by an amidopyridinate ligand: synthesis, characterization and catalytic performance in isoprene polymerization, hydroelementation and carbon dioxide hydrosilylation**

For your information: You can cite this article before you receive notification of the page numbers by using the following format: (authors), Dalton Trans., (year), DOI: 10.1039/c9dt04338a.

Editor's queries are marked like this Q1, Q2, and for your convenience line numbers are indicated like this 5, 10, 15, ...

Please ensure that all queries are answered when returning your proof corrections so that publication of your article is not delayed.

Query Reference	Query	Remarks
Q1	Funder details have been incorporated in the funder table using information provided in the article text. Please check that the funder information in the table is correct.	Thanks, all details are correct
Q2	Please check that the inserted CCDC numbers are correct.	CCDC numbers are correct, thanks!
Q3	Please confirm that the spelling and format of all author names is correct. Names will be indexed and cited as shown on the proof, so these must be correct. No late corrections can be made.	All names are correct, thanks!
Q4	Do you wish to add an e-mail address for the corresponding author? If so, please provide the relevant information.	emails are provided in notes directly on the manuscript below (Q4)
Q5	Please explain the significance of superscript "o" used in Table 2. If this is intended to be a link to a footnote then please provide the appropriate text.	Please, remove "o" superscript from the table. The heading should be simply "TOF". Thanks.
Q6	Text has been provided for footnote a in Table 3, but there does not appear to be a corresponding citation in the table. Please indicate a suitable location for the footnote citation.	comments are given in table heading (see below for details) "Q6"
Q7	Ref. 33: Please check that the initials for the 2nd author are displayed correctly.	comments are given in reference 33 "Q7"
Q8	Ref. 33: Please provide the last name for the 2nd author.	comments are given in reference 33 "Q8"
Q9	Ref. 39: Please provide the last name for the 1st editor.	comments are given in reference 39 "Q9"

Dalton Transactions

ROYAL SOCIETY OF CHEMISTRY

PAPER

Bis(alkyl) scandium and yttrium complexes coordinated by an amidopyridinate ligand: synthesis, characterization and catalytic performance in isoprene polymerization, hydroelementation and carbon dioxide hydrosilylation†

Cite this: DOI: 10.1039/c9dt04338a

G. A. Gurina, [a] A. A. Kissel,[a,b] D. M. Lyubov, [a] L. Luconi,[c] A. Rossin,[c] G. Tuci,[c] A. V. Cherkasov, [a] K. A. Lyssenko,[a] A. S. Shavyrin,[a] A. M. Ob'edkov,[a] G. Giambastiani *[c,d,e] and A. A. Trifonov *[a,b]

New neutral bis(alkyl) Sc and Y complexes [N,N^{py},N^{-}]Ln(CH$_2$SiMe$_3$)$_2$(THF)$_n$ [n = 0, Ln = Sc (**1$_{Sc}$**), Y (**1$_Y$**); n = 1, Ln = Y (**1$_Y^{THF}$**)] stabilized by a tridentate monoanionic amidopyridinate ligand were straightforwardly prepared by alkane elimination, upon mixing ligand [N,N^{py},N^{-}]H and metal precursor Ln(CH$_2$SiMe$_3$)$_3$(THF)$_2$ in toluene at 0 °C. Depending on the work-up conditions, yttrium bis(alkyl)s were isolated as either a pentacoordinate Lewis base free complex [N,N^{py},N^{-}]Y(CH$_2$SiMe$_3$)$_2$ (**1$_Y$**) or as a hexacoordinate THF adduct [N,N^{py},N^{-}]Y(CH$_2$SiMe$_3$)$_2$THF (**1$_Y^{THF}$**). For the smaller Sc ion the only solvent-free complex [N,N^{py},N^{-}]Y(CH$_2$SiMe$_3$)$_2$ (**1$_{Sc}$**) was isolated as a pentacoordinate species irrespective of the reaction/work-up/crystallization conditions applied. Complexes **1$_{Ln}$** (Ln = Y, Sc) and **1$_Y^{THF}$** were scrutinized as pre-catalysts in ternary catalytic systems Ln/borate/Al^{i}Bu$_3$ (borate = [HNMe$_2$Ph][B(C$_6$F$_5$)$_4$] or [Ph$_3$C][B(C$_6$F$_5$)$_4$]), applied to isoprene (IP) polymerization, providing moderate activity albeit high selectivity with predominant formation of 1,4-*cis* polyisoprene (up to 99%). The same complexes proved to be effcient catalysts also for the intermolecular hydrolelementation of styrene with various EH sustrates (pyrrolidine, morpholine, Ph$_2$PH, PhPH$_2$, PhSH) affording linear anti-Markovnikov addition products exclusively. After a preliminary activation by B(C$_6$F$_5$)$_3$, selected bis(alkyl) complexes from this series have been finally used as valuable pre-catalysts for the CO$_2$ hydrosylilation to CH$_4$ in the presence of organosilanes as reducing agents (PhMe$_2$SiH, PhSiH$_3$, Et$_2$MeSiH).

Received 8th November 2019,
Accepted 3rd December 2019

DOI: 10.1039/c9dt04338a

rsc.li/dalton

Introduction

Rare-earth bis(alkyl) complexes have received a great deal of attention in the last decades because of their unique reactivity[1–9] which enables hardly implementable transformations such as activation of generally inert sp^3- and sp^2-hybridized C–H bonds of hydrocarbons.[10–14] Extensive research efforts have revealed the great potentiality of rare-earth metal alkyl derivatives as catalysts (or pre-catalysts) for a variety of hydroelementation reactions of multiple C–C bonds (hydrosilylation reaction;[15–21] intra- and inter-molecular hydroamination,[15,22–28] hydrophosphination;[29] hydrobenzylation and hydroarylation).[30–35] In addition, cationic mono (alkyl) rare-earth complexes[36,37] have emerged as valuable candidates for promoting the catalytic homo- and co-polymerization of olefins and dienes[36–63] thus providing an important boost to the development of the field.

The relatively large ion size of rare-earth metals, their electropositivity along with the limited covalent nature of metal–ligand bonding in these coordination compounds play a decisive role in controlling both stability and chemical reactivity of

[a]Institute of Organometallic Chemistry of Russian Academy of Sciences, Tropinina str. 49, GSP-445, 603950 Nizhny Novgorod, Russia
[b]Institute of Organoelement Compounds of Russian Academy of Sciences, Vavilova str. 28, 119334 Moscow, Russia
[c]Institute of Chemistry of OrganoMetallic Compounds, ICCOM-CNR and Consorzio INSTM, Via Madonna del Piano, 10-50019, Sesto F.no, Florence, Italy
[d]Institute of Chemistry and Processes for Energy, Environment and Health (ICPEES), UMR 7515 CNRS – University of Strasbourg (UdS), 25, rue Becquerel, 67087 Strasbourg Cedex 02, France
[e]Kazan Federal University, 420008 Kazan, Russian Federation

† Electronic supplementary information (ESI) available. CCDC 1956756–1956758. For ESI and crystallographic data in CIF or other electronic format see DOI: 10.1039/c9dt04338a

these species. Hence, the design and synthesis of tailored ancillary ligands suitable for coordination to rare-earth ions, the isolation of the corresponding alkyl species and the investigation of their complex structure–reactivity relationship are currently one of the main trends in organo-rare-earth chemistry. This fundamental study is important to gain insights on the fine tuning of their reactivity as homogeneous catalysts.

The paper describes the synthesis and characterization of three neutral bis(alkyl)-organolanthanide complexes supported by a tridentate {*N*,*N*,*N*$^-$} monoanionic amidopyridinate ligand and their high versatility in catalysis. Indeed, these coordination compounds have been scrutinized as catalysts or catalyst precursors in a variety of highly challenging transformations. As a first trial, [N,N^{py},N$^-$]Ln(CH$_2$SiMe$_3$)$_2$(THF)$_n$ [n = 0, Ln = Sc (**1$_{Sc}$**), Y (**1$_Y$**); n = 1, Ln = Y (**1$_Y^{THF}$**)] were tested as pre-catalysts for the stereospecific polymerization of 1,3-conjugated dienes. We focused on the isoprene (IP) polymerization, one of the most investigated and industrially relevant processes for the preparation of polyisoprenes (PIPs) with controlled microstructures.[41,42,44,49–52,64–71] All catalytic systems showed fairly good activity in the process with a prevalent *cis*-1,4 monomer enchainment in the polymers microstructure, irrespective to the nature of the rare-earth ion at work. With the aim of widening the catalysts scope, the bis(alkyl) organolanthanide complexes from this series have also been tested as catalysts for the intermolecular styrene hydro-elementation reaction in the presence of a variety of nucleophiles. Synthesis of phosphorus-, nitrogen- and sulfur-containing organic molecules from unsaturated compounds certainly covers one of the major domains of organolanthanides in catalysis. Hydroelementation (or hydrofunctionalization) consists in the formal and metal-mediated addition of an E–H bond (E = P, N, S) on a carbon–carbon multiple bond. It represents a highly efficient, sustainable and environmentally friendly methodology for the preparation of organic commodities. In this context, the choice of a tailored catalyst allows for the control of the regio-, chemo- and stereo-selectivity of the addition products.

Finally, to further extend the application range of these species, selected complexes from this series have been employed as pre-catalysts for CO_2 activation and its subsequent hydrosilylation to methane (CH_4). Cationic early-transition-metal complexes have already been scrutinized as active catalysts for the process in combination with a variety of hydrosilanes. Matsuo and Kawaguchi reported firstly on the use of Zr^{IV} dialkyl phenoxide complexes in combination with B(C$_6$F$_5$)$_3$ as a strong Lewis acid for the tandem CO_2 hydrosilylation to CH_4.[72] Since their seminal work, other transition metal complexes[73–75] and organolanthanides[76,77] have been exploited for the tandem transformation. In particular, we have recently described the tandem hydrosilylation catalysis with a new class of group-IV coordination compounds stabilized by a tridentate κ^3\{*N*$^-$,*N*,*N*$^-$\} ligand, using B(C$_6$F$_5$)$_3$ as activator/co-catalyst.[78] With TOF values up to twice than those claimed for the benchmark dialkyl phenoxide Zr^{IV}-complex, our κ^3\{*N*$^-$,*N*,*N*$^-$\}Zr^{IV} species was found to rank among the systems with the highest catalytic performance in the tandem hydrosilylation process compared to related catalysts from the state-of-the-art.

A comprehensive overview of all catalytic issues with the newly synthesized organolanthanides complexes has been detailed afterwards.

Results and discussion

Synthesis and characterization of bis(alkyl) complexes 1$_{Sc}$, 1$_Y$ and 1$_Y^{THF}$

Bis(alkyl) scandium and yttrium derivatives **1$_{Sc}$**, **1$_Y$** and **1$_Y^{THF}$** coordinated by the tridentate κ^3\{*N*,*N*,*N*$^-$\} amidopyridinate ligand **1** were straightforwardly synthesized through alkane elimination from an equimolar mixture of ligand **1** and the tris(alkyl) metal precursor of choice [Ln(CH$_2$SiMe$_3$)$_3$(THF)$_2$; Ln = Sc, Y] (Scheme 1).

Complexes **1$_Y$**, **1$_Y^{THF}$** and **1$_{Sc}$** were isolated as highly air- and moisture-sensitive brownish-red (**1$_Y$**, **1$_Y^{THF}$**) or dark red (**1$_{Sc}$**) crystals in 79, 74 and 83% yields, respectively. Depending on the hydrocarbon solvent used [toluene (i) *vs.* hexane (ii)], different coordination compounds have been isolated using Y(CH$_2$SiMe)$_3$(THF)$_2$ as metal precursor. Indeed, the slow crystallization from cold toluene gave the pentacoordinate complex **1$_Y$**, while no crystals were obtained from pure cold hexane. Crystals suitable for X-ray diffraction analysis could only be obtained upon addition of few drops of THF (hexane : THF = 4 : 1 *ca.*) as to afford the hexacoordinated THF-adduct **1$_Y^{THF}$**. As for the scandium complex, the only solvent-free complex **1$_{Sc}$** was isolated as a pentacoordinate species irrespective to the applied reaction/crystallization conditions. Indeed, the smaller scandium ion size did not show any modification of the complex coordination sphere as a function of the crystallization solvent used (toluene *vs.* hexane/THF).

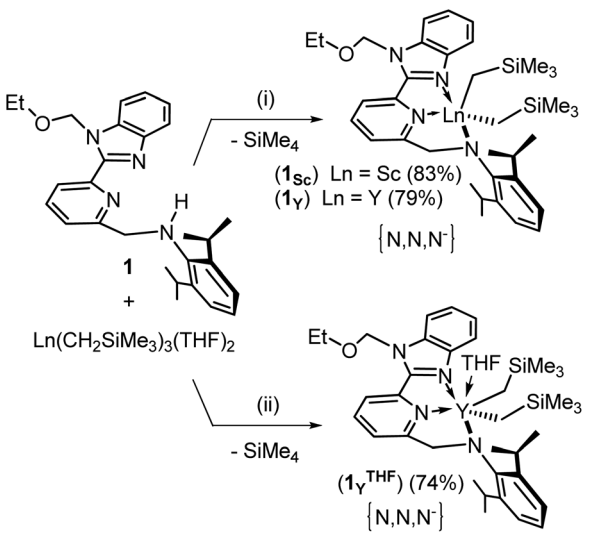

Scheme 1 Synthesis of bis(alkyl) complexes **1$_{Ln}$** (Ln = Sc, Y) and **1$_Y^{THF}$**. (i) Toluene, 0 °C; (ii) hexane, 0 °C followed by hexane/THF recrystallization.

All isolated compounds have shown excellent stability in dry and degassed benzene-d_6 solution at ambient temperature with no apparent decomposition per weeks. It should be noticed that related yttrium bis(alkyl) coordination compounds formerly reported by us and featured by benzothiazole substituted amidopyridinate $\kappa^3\{N,N,N^-\}$ ligands underwent rapid ligand C–S bond cleavage upon treatment with THF, to give compounds with original and unexpected coordination environments.[79] At odds with benzothiazole substituted $\kappa^3\{N,N,N^-\}$ ligands, no traces of new species due to the imidazole ring-opening were observed either with $\mathbf{1_Y}$ or $\mathbf{1_Y}^{\mathbf{THF}}$, even after keeping the latter under harsh conditions for prolonged times (benzene-d_6 at 60 °C for 24 h). The higher chemical stability of the benzoimidazole ligand is ascribed to the relatively higher energy required for the C–N bond cleavage (72.9 kcal mol^{-1}, 305 kJ mol^{-1}) compared to that required for breaking the C–S bond (61.9 kcal mol^{-1}, 259 kJ mol^{-1}).[80] The ^{1}H NMR spectra recorded for all complexes show largely superimposable regions with well distinct set of signals (see Experimental section for NMR details and Fig. S1, S3, and S5†). In particular, the methylene protons at the two residual –CH_2SiMe_3 fragments in $\mathbf{1_{Sc}}$ and $\mathbf{1_Y}$ and $\mathbf{1_Y}^{\mathbf{THF}}$ are diastereotopic and appear as two doublets ($\mathbf{1_{Sc}}$ δ_H = 0.31 and 0.65 ppm, $^2J_{HH}$ = 11.3 Hz; $\mathbf{1_Y}$ δ_H = −0.10 and 0.13 ppm, $^2J_{HH}$ = 10.7 Hz; $\mathbf{1_Y}^{\mathbf{THF}}$ δ_H = −0.67 and −0.60 ppm, $^2J_{HH}$ = 10.7 Hz). Carbons from the same methylene fragments give rise to a slightly broadened singlet in $^{13}C\{^1H\}$ NMR spectrum of $\mathbf{1_{Sc}}$ at δ_C = 39.1 ppm, while doublets are given for $\mathbf{1_Y}$ (δ_C = 34.0 ppm, $^1J_{YC}$ = 38.5 Hz) and $\mathbf{1_Y}^{\mathbf{THF}}$ (δ_C = 26.7 ppm, $^1J_{YC}$ = 33.7 Hz), respectively (see Experimental section for NMR details and Fig. S2, S4, and S6†).

Notably, the presence of a coordinated electron donating THF molecule in $\mathbf{1_Y}^{\mathbf{THF}}$ causes a significant modification of the ^{1}H and ^{13}C NMR chemical shifts.

Indeed, the above-mentioned methylene fragments on $\mathbf{1_Y}^{\mathbf{THF}}$ are significantly shifted with respect to its THF-free ($\mathbf{1_Y}$) counterpart. 2D ^{1}H–^{89}Y MHQC correlation spectra reveal the same trend for the chemical shifts of ^{89}Y nuclei in the two coordination compounds $\mathbf{1_Y}$ and $\mathbf{1_Y}^{\mathbf{THF}}$. As spectra on Fig. S7 show (see the ESI†), ^{89}Y in $\mathbf{1_Y}^{\mathbf{THF}}$ is markedly shifted to upper field (singlet at 801 ppm) compared to its THF-free counterpart $\mathbf{1_Y}$ (singlet at 1033 ppm). Finally, trimethylsilyl groups of alkyl ligands, pyridine-amido bridging methylene fragments and N–CH_2–O moieties of the N-protecting groups give rise sharp singlets in the ^{1}H and $^{13}C\{^1H\}$ NMR spectra {[$Si(CH_3)_3$: δ_H = 0.01 ppm and δ_C = 3.6 ppm for $\mathbf{1_{Sc}}$; δ_H = 0.07 ppm and δ_C = 3.7 ppm for $\mathbf{1_Y}$; δ_H = −0.25 ppm and δ_C = 3.7 ppm for $\mathbf{1_Y}^{\mathbf{THF}}$] [Py–$CH_2$–N: δ_H = 4.92 ppm and δ_C = 64.9 ppm for $\mathbf{1_{Sc}}$; δ_H = 4.97 ppm and δ_C = 65.5 ppm for $\mathbf{1_Y}$; δ_H = 5.00 ppm and δ_C = 66.0 ppm for $\mathbf{1_Y}^{\mathbf{THF}}$] [N–$CH_2$–O: δ_H = 4.82 ppm and δ_C = 73.1 ppm for $\mathbf{1_{Sc}}$; δ_H = 4.79 ppm and δ_C = 72.9 ppm for $\mathbf{1_Y}$; δ_H = 5.10 ppm and δ_C = 72.8 ppm for $\mathbf{1_Y}^{\mathbf{THF}}$]}. The solid-state structures of complexes $\mathbf{1_{Sc}}$, $\mathbf{1_Y}$ and $\mathbf{1_Y}^{\mathbf{THF}}$ have been obtained through single crystal X-ray diffraction analysis and a perspective view of each molecule is given in Fig. 1–3. Table 1 summarizes selected bond lengths and angles of all structures while all the main crystal and structural refinement data are

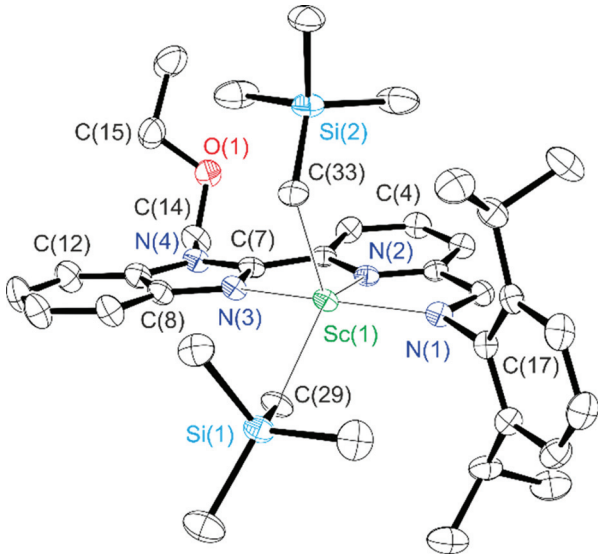

Fig. 1 Molecular structure of $\mathbf{1_{Sc}}$. Thermal ellipsoids are drawn at the 30% probability level. Hydrogen atoms are omitted for clarity.

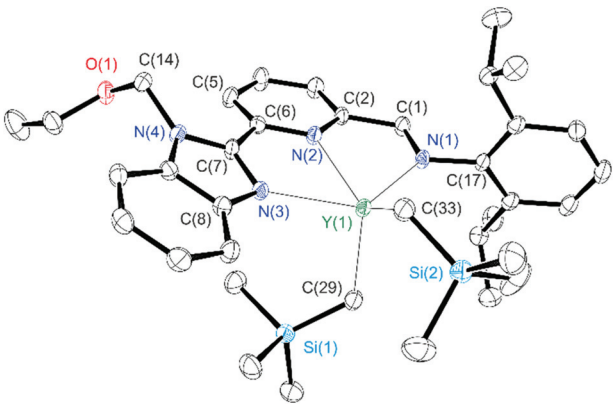

Fig. 2 Molecular structure of $\mathbf{1_Y}$. Thermal ellipsoids are drawn at the 30% probability level. Hydrogen atoms are omitted for clarity.

provided in Table S1 (see ESI†). Five-coordinated complexes $\mathbf{1_{Sc}}$ and $\mathbf{1_Y}$ crystallize in monoclinic $P2_1/c$ and C_2/c space groups in a distorted square-pyramidal coordination geometry,[81] in the form of solvates with 1 and $1\frac{1}{2}$ molecules of toluene, respectively. Complex $\mathbf{1_Y}^{\mathbf{THF}}$ crystallizes in the triclinic $P\bar{1}$ space group as a distorted hexacoordinated compound, solvated with $\frac{1}{2}$ molecule of hexane. For all complexes, the amidopyridinate ligand acts as tridentate $\kappa^3\{N,N,N^-\}$ monoanionic species with one covalently linked amido nitrogen and two coordinative N-donor sites to the rare-earth metal ion. Similar coordination environments have already been reported in the literature for related bis(alkyl) organolanthanides[79] and group-IV transition metal complexes.[78]

The different radii of the two metal ions as well as their different coordination number are found to affect the geometry of the metal-amidopyridinate fragment. Thus, in $\mathbf{1_{Sc}}$ the amidopyridinate ligand is nearly planar with a dihedral angle between the benzoimidazolyl and pyridyl planes of 8.0(2)°. The

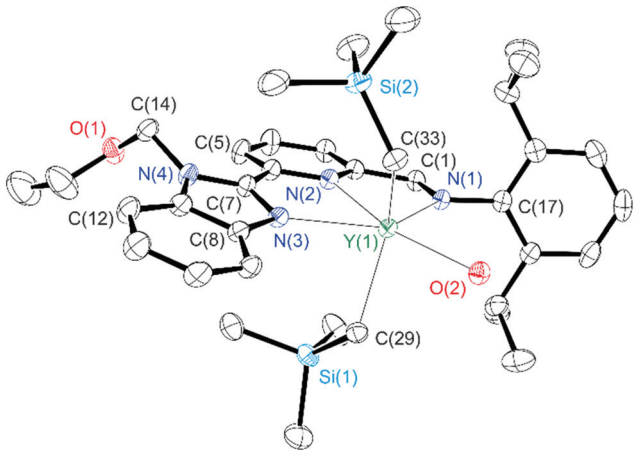

Fig. 3 Molecular structure of $\mathbf{1_Y}^{THF}$. Thermal ellipsoids are drawn at the 30% probability level. Hydrogen atoms and THF molecule (except for the coordinating O(2) atom are omitted for clarity.

Table 1 Selected bond distances (Å) and angles (°) for complexes $\mathbf{1_{Sc}}$, $\mathbf{1_Y}$ and $\mathbf{1_Y}^{THF}$

	$\mathbf{1_{Sc}}\cdot MeC_6H_5$	$\mathbf{1_Y}\cdot 1\frac{1}{2}MeC_6H_5$	$\mathbf{1_Y}^{THF}\cdot\frac{1}{2}C_6H_{14}$
Ln–C(29)	2.250(3)	2.396(3)	2.463(2)
Ln–C(33)	2.226(3)	2.424(3)	2.475(2)
Ln–N(1)	2.081(2)	2.240(2)	2.267(2)
Ln–N(2)	2.284(2)	2.452(2)	2.486(2)
Ln–N(3)	2.303(2)	2.456(2)	2.485(2)
Ln–O(1)	—	—	2.441(2)
N(1)–C(1)	1.448(3)	1.447(4)	1.443(3)
C(1)–C(2)	1.493(3)	1.506(4)	1.495(3)
N(2)–C(2)	1.331(3)	1.335(4)	1.334(3)
N(2)–C(6)	1.362(3)	1.363(4)	1.362(3)
C(6)–C(7)	1.468(4)	1.477(4)	1.473(3)
N(3)–C(7)	1.328(3)	1.329(4)	1.318(3)
N(3)–C(8)	1.390(3)	1.398(4)	1.388(3)
N(1)–Ln(1)–N(2)	72.79(8)	68.18(8)	67.71(6)
N(2)–Ln(1)–N(3)	68.94(7)	65.72(8)	64.57(6)
N(1)–Ln(1)–C(29)	105.57(9)	106.74(2)	110.99(7)
N(1)–Ln(1)–C(33)	110.35(9)	108.9(2)	115.22(7)
N(2)–Ln(1)–C(29)	132.46(9)	111.7(2)	102.58(7)
N(2)–Ln(1)–C(33)	108.77(9)	132.6(2)	109.19(7)
N(3)–Ln(1)–C(29)	93.47(9)	99.9(2)	80.69(7)
N(3)–Ln(1)–C(33)	90.90(9)	94.5(2)	80.45(7)

Sc^{III} ion deviates of only 0.3 Å from the plane intercepted by the $\{N,N,N^-\}$ tridentate ligand. The bigger metal ion size (Y^{III} *vs.* Sc^{III}) increases the dihedral angle between the benzoimidazolyl and pyridyl planes, with values up to 18.6(2)° and 13.5(2)° for $\mathbf{1_Y}$ and $\mathbf{1_Y}^{THF}$, respectively.

The Ln–C (2.226(3) and 2.250(3) Å) and Ln–N (Sc–N_{amido} 2.081(2); Sc–N_{py} 2.284(2), Sc–$N_{imidazol}$ 2.303(2) Å) distances in $\mathbf{1_{Sc}}$ proved to be in a good agreement with the distances measured in the related Sc bis(alkyl) complexes with various $\kappa^3\{N,N,N\}$ tridentate ligands.[52,70,82–86] As expected, in the six-coordinated $\mathbf{1_Y}^{THF}$ complex, Y–C (2.475(2) and 2.463(2) Å) and Y–N (Y–N_{amido} 2.267(2), Y–N_{py} 2.486(2), Y–$N_{imidazol}$ 2.485(2) Å) bond distances are slightly longer compared to those measured for the pentacoordinate $\mathbf{1_Y}$ (Y–C 2.424(3) and 2.396(3) Å, Y–N_{amido} 2.240(2), Y–N_{py} 2.452(2), Y–$N_{imidazol}$ 2.456(2) Å).

However, the values fall in the typical range given for related five- and six-coordinate yttrium bis(alkyl) species containing tridentate $\kappa^3\{N,N,N^-\}$ monoanionic amidopyridinate ligands.[79]

Study of the catalytic performance of complexes $\mathbf{1_{Sc}}$, $\mathbf{1_Y}$ and $\mathbf{1_Y}^{THF}$

Isoprene polymerization tests. The stereospecific diene polymerization is an area of catalysis where organolanthanides have largely been employed with success, demonstrating all their inherent potentiality. On this regard, the bis(alkyl) compounds $\mathbf{1_{Sc}}$, $\mathbf{1_Y}$ and $\mathbf{1_Y}^{THF}$ have been initially scrutinized as catalyst precursors for the isoprene (IP) polymerization under variable reaction conditions. The choice of metal ion and the catalyst activator(s) play a fundamental role on the control of the ultimate catalyst performance as well as on the microstructure of the resulting polymers. As Table 2 shows, neutral bis(alkyl) complexes $\mathbf{1_{Sc}}$, $\mathbf{1_Y}$ and $\mathbf{1_Y}^{THF}$ as well as their binary mixtures $\mathbf{1_{Ln}}$/borate [borate = $[Ph_3C][B(C_6F_5)_4]$ (TB) or $[PhNHMe_2][B(C_6F_5)_4]$ (HNB)] or $\mathbf{1_{Ln}}/Al^iBu_3$ did not show any appreciable activity in the process even at temperature higher than ambient (Table 2, entries 1–3). On the other hand, ternary mixtures $\mathbf{1_{Ln}}$/borate/Al^iBu_3 (1 : 1 : 10 molar ratio) suddenly trigger the isoprene polymerization with fairly good catalytic activity and selectivity depending from the catalyst/activator system used (*vide infra*). In the case of $\mathbf{1_{Sc}}$, its catalytic performance was found to be independent from the choice of the borate co-reagent in the ternary mixture (TB *vs.* HNB) with an almost complete isoprene conversion (1000 eq. *vs.* cat.) after 6 h on run (Table 2, entries 4–7). At odds with $\mathbf{1_{Sc}}$, the yttrium counterpart $\mathbf{1_Y}$ showed a marked dependence of its catalytic performance from the nature of activator used in the tertiary mixture. Indeed, when HNB was used as activator a marked slowdown of the catalyst' performance was observed with a monomer conversion close to quantitative (96%) only after 18 reaction hours (Table 2, entry 8). This result is in clear-cut contrast with the faster and quantitative monomer conversion achieved with the $\mathbf{1_Y}$/TB/Al^iBu_3 tertiary system at work (Table 2, entry 9). Indeed, the latter ranks among the most performing complexes of this series reported so far in the literature and applied to IP polymerization. The worse performance of the tertiary $\mathbf{1_Y}$/HNB/Al^iBu_3 system is attributed to the evolution of the nucleophilic *N*,*N*-dimethyl aniline side-product whose subsequent and detrimental competition with isoprene for the coordination to the electrophilic metal ion offers a reasonable explanation to the observed reaction slowdown.[87,88] Notably, such a borate effect on the catalyst's performance was found to be less pronounced in the case of the THF-containing species $\mathbf{1_Y}^{THF}$ (Table 2, entries 10–13). Indeed, a quantitative isoprene conversion was achieved with the $\mathbf{1_Y}^{THF}$/borate/Al^iBu_3 tertiary system after 6 and 7 hours with TB and HNB as activator, respectively (Table 2, entries 11 and 13). If a more sterically crowded metal coordination sphere ($\mathbf{1_Y}^{THF}$ *vs.* $\mathbf{1_Y}$) results into an appreciable drop of the catalyst turn-over-frequency (TOF) (Table 2, entries 9 *vs.* 12), the presence of a THF molecule coordinated to the metal ion partially prevents the competitive/

Table 2 Isoprene polymerization data and polymer characterization[a]

Entry	Cat.	Activ./Al^{i}Bu$_3$ (eq.)	t [h]	Yield[b] [%]	TOF	Microstructure[c] (%)			M_n[d] [10^{-4}]	M_w/M_n[d]
						trans-1,4	*cis*-1,4	3,4-Motif		
1[e]	$\mathbf{1_{Ln}}$	—/—	6	0	—	—	—	—	—	—
2[e]	$\mathbf{1_{Ln}}$	TB or HNB/—	6	0	—	—	—	—	—	—
3[e]	$\mathbf{1_{Ln}}$	—/(10)	6	0	—	—	—	—	—	—
4	$\mathbf{1_{Sc}}$	HNB/(10)	5	89	178.0	—	n.d.	n.d.	n.d.	n.d.
5	$\mathbf{1_{Sc}}$	HNB/(10)	6	>99	—	—	75.2	24.8	6.1	1.16
6	$\mathbf{1_{Sc}}$	TB/(10)	5	92	184.0	—	n.d.	n.d.	n.d.	n.d.
7	$\mathbf{1_{Sc}}$	TB/(10)	6	>99	—	—	87.9	12.1	5.2	1.17
8	$\mathbf{1_{Y}}$	HNB/(10)	18	96	53.3	—	90.2	9.8	9.8	1.97
9	$\mathbf{1_{Y}}$	TB/(10)	2	92	460.0	—	92.4	7.6	11.1	2.13
10	$\mathbf{1_{Y}^{THF}}$	HNB/(10)	6	94	156.7	—	n.d.	n.d.	n.d.	n.d.
11	$\mathbf{1_{Y}^{THF}}$	HNB/(10)	7	>99	—	—	75.9	24.1	5.2	2.14
12	$\mathbf{1_{Y}^{THF}}$	TB/(10)	5	92	184.0	—	n.d.	n.d.	n.d.	n.d.
13	$\mathbf{1_{Y}^{THF}}$	TB/(10)	6	>99	—	—	98.0	2.0	11.3	2.81

[a] Polymerization conditions: Temp = rt (20–22 °C); toluene (3.5 mL); 10 mmol of IP [IP]; 10 μmol of catalyst [cat.] ($\mathbf{1_{Ln}}$); [cat.] : [IP] = 1 : 1000; activators: TB, [Ph$_3$C][B(C$_6$F$_5$)$_4$]; HNB, [PhNHMe$_2$][B(C$_6$F$_5$)$_4$]; [cat.] : [activator] = 1 : 1.05. [b] Average value calculated over three independent runs. [c] Determined by ^{1}H NMR and ^{13}C{^{1}H} NMR spectroscopy in CDCl$_3$ at rt. [d] Determined by GPC in THF at 40 °C against a polystyrene standard. [e] Polymerization runs performed at either rt (20–22 °C) or 50 °C.

poisoning effect raising from the nucleophilic *N*,*N*-dimethyl aniline by-product (Table 2, entries 8 *vs.* 11). As for the composition of produced polyisoprenes (PIPs), $\mathbf{1_{Sc}}$ provides samples featured by narrow molecular weight distribution (M_w/M_n) regardless the nature of the cationizing agent used in the mixture (Table 2, entries 5 and 7). On the other hand, both yttrium systems gave polymers with relatively broader molecular weight distribution (M_w/M_n = 1.97–2.81). In terms of polymer microstructures, all TB and HNB activated complexes from this series display similar microstructures, prevalently made of 1,4-*cis* units and 3,4-motif as determined *via* ^{1}H and ^{13}C{^{1}H} NMR spectroscopy (see Fig. S8–S15†). No 1,4-*trans* units were observed in all synthesized and isolated PIPs. The catalytic systems based on yttrium provided 1,4-*cis* selectivity as higher as 98% as a function of the yttrium precursor and the activator used. $\mathbf{1_{Y}^{THF}}$/borate/Al^{i}Bu$_3$ have shown the highest differences on the microstructure of the produced PIPs depending on the borate used. While TB gave a PIP with the 1,4-*cis* selectivity that was among the highest given for this class of compounds (98%), the use of HNB as activator translated into a polymer with a 1,4-*cis* selectivity lying around 76%. The pentacoordinate $\mathbf{1_{Y}}$ afforded PIPs with similar contents of 1,4-*cis* units and irrespective to the nature of the activator used (Table 2, entries 8 and 9). Finally, $\mathbf{1_{Sc}}$ displayed lower 1,4-*cis* stereospecificity in the isolated PIPs. Indeed, a 1,4-*cis* content ranged from 75.2 to 87.9% as a function of the activator used in the ternary system (Table 2, entries 5 and 7).

Hydroelementation runs for intermolecular C–N, C–S and C–P bond forming reactions

To widen the application range of the newly synthesized organolanthanides, all complexes from this series were tested as pre-catalysts for the intermolecular C–N, C–S and C–P bond forming reactions on unsaturated hydrocarbons (hydroelementation process).[29] For these trials, styrene was selected as the probe molecule to be used in combination with amines, phosphines and thiols. Organolanthanides are known to catalyse these efficient and atom-saving processes for the production of heteroatom-containing compounds through the formal addition of an E–H bond (E = N, P, S) to multiple C–C bonds.[29] The catalytic tests on intermolecular styrene hydroelementations were run under solvent-free conditions, using neat substrate mixtures in the presence of 2 mol% of each bis(alkyl) pre-catalysts at 70 °C ([styrene]/[E–H]/[**Ln**] = 50/50/1). As a preliminary screening, each catalytic run was conventionally carried out for 48 h without any optimization of the reaction time. Scheme 2 outlines the hydroelementation processes investigated with the $\mathbf{1_{Ln}}$ from this catalysts series while Table 3 lists the corresponding conversions and (whenever applicable) process selectivity.

All bis(alkyl) pre-catalysts from the synthesized series turned out to be suitable candidates to mediate these reactions under relatively mild conditions, showing complete regioselectivity with the generation of the unique anti-Markovnikov addition product regardless of the nature of the E–H reagent chosen. As for the intermolecular hydroamination, pyrrolidine

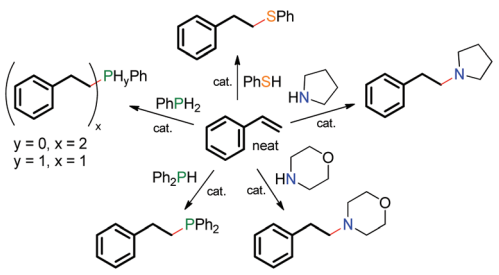

Scheme 2 General scheme for the styrene hydroelementation catalyzed by complexes $\mathbf{1_{Ln}}$ with a series of E–H (E = N, P, S) reagents. Reaction conditions: Neat reagents, ([styrene]/[EH]/[**Ln**] = 50/50/1), 70 °C, 48 h.

Table 3 Styrene hydroelementation catalyzed by complexes $\mathbf{1}_{Ln}$

Entry	Cat.	E–H	Conv.[b] (%)	Selectivity Mono-/Di-hydroelem.[b]
1	$\mathbf{1}_{Sc}$	$(CH_2)_4NH$	63	n.a.
2	$\mathbf{1}_{Y}$	$(CH_2)_4NH$	76	n.a.
3	$\mathbf{1}_{Y}^{THF}$	$(CH_2)_4NH$	44	n.a.
4	$\mathbf{1}_{Sc}$	$O(CH_2)_4NH$	—	n.a.
5	$\mathbf{1}_{Y}$	$O(CH_2)_4NH$	37	n.a.
6	$\mathbf{1}_{Y}^{THF}$	$O(CH_2)_4NH$	33	n.a.
7	$\mathbf{1}_{Sc}$	$PhPH_2$	95	78/22
8	$\mathbf{1}_{Y}$	$PhPH_2$	99	84/16
9	$\mathbf{1}_{Y}^{THF}$	$PhPH_2$	99	81/19
10	$\mathbf{1}_{Sc}$	Ph_2PH	90	n.a.
11	$\mathbf{1}_{Y}$	Ph_2PH	99	n.a.
12	$\mathbf{1}_{Y}^{THF}$	Ph_2PH	99	n.a.
13	$\mathbf{1}_{Sc}$	PhSH	95	n.a.
14	$\mathbf{1}_{Y}$	PhSH	99	n.a.
15	$\mathbf{1}_{Y}^{THF}$	PhSH	99	n.a.
16	$\mathbf{1}_{Sc}$	CySH	0	n.a.
17	$\mathbf{1}_{Y}$	CySH	0	n.a.
18	$\mathbf{1}_{Y}^{THF}$	CySH	0	n.a.

[a] Reaction conditions: Temp = 70 °C; neat reagents, [styrene]/[E–H]/[**Ln**] = 50/50/1 = 0.5 mmol/0.5 mmol/10 μmol, 48 h. [b] Determined by ^{1}H and $^{13}C\{^1H\}$ NMR or $^{31}P\{^1H\}$ spectroscopy in $CDCl_3$. n.a. = not applicable.

and morpholine were selected as benchmark reagents for the $\mathbf{1}_{Ln}$ mediated addition to styrene. As Table 3 shows, complex $\mathbf{1}_{Y}$ was the most active from this series with styrene conversions of 76% and 37% for the pyrrolidine and morpholine adducts, respectively (Table 3, entries 2 and 5). Conversions measured under identical conditions but in the presence of the six-coordinated $\mathbf{1}_{Y}^{THF}$ were affected by the more crowded metal coordination sphere. Indeed, the presence of a THF molecule coordinated to the metal ion was supposed to limit the regular uptake of the substrate to the catalyst active site. As a result, hydroamination adducts with pyrrolidine and morpholine were formed in only 44% and 33% yield, respectively (Table 3, entries 3 and 6). The $\mathbf{1}_{Sc}$ showed lower catalytic performance compared to its yttrium pentacoordinate counterpart. Indeed, it afforded 63% styrene conversion in the pyrrolidine adduct (Table 3, entry 1) whereas it did not show any appreciable catalytic activity when morpholine was employed as reagent. $\mathbf{1}_{Sc}$ was completely inactive for the intermolecular hydroamination using morpholine as reagent thus confirming the following catalysts' trend in the process: $\mathbf{1}_{Y} > \mathbf{1}_{Y}^{THF} \ggg \mathbf{1}_{Sc}$. All catalysts were also investigated in the hydrophosphination reaction using phenylphosphine ($PhPH_2$) and diphenylphosphine (Ph_2PH) as probe reagents for the addition to styrene. Similarly to hydroamination reactions, all catalyzed reactions with the two phosphines resulted into regioselective anti-Markovnikov addition products only. However, when $PhPH_2$ was used as reagent the chemoselectivity (mono- *vs.* dihydrophosphination reaction) turned out to be moderate. Indeed, with all complexes from this series the combination of styrene with $PhPH_2$ in equimolar amount afforded mixtures of secondary and tertiary phosphines with the former being always predominant (from 78–84%) (Table 3, entries 7–9). With both phosphines, the reactions catalysed by $\mathbf{1}_{Y}$ and $\mathbf{1}_{Y}^{THF}$ provided, after 48 h at 70 °C, quantitative styrene conversions (Table 3, entries 8, 9 and 11, 12) whereas a slightly lower activity was given with the $\mathbf{1}_{Sc}$ complex at work (Table 3, entries 7 and 10).

As a last hydroelementation trial, complexes $\mathbf{1}_{Sc}$, $\mathbf{1}_{Y}$ and $\mathbf{1}_{Y}^{THF}$ were scrutinized as catalysts for the intermolecular styrene hydrothiolation using thiophenol (PhSH) and cyclohexanethiol (CySH) as probe reagent molecules. As Table 3 shows, all complexes catalyzed the PhSH-styrene hydrothiolation in regioselective fashion (anti-Markovnikov addition) with from excellent to quantitative yields (Table 3, entries 13–15). Notably, no catalytic activity was observed when the same reactions were carried out with the aliphatic thiol (CySH) (Table 3, entries 16–18). Such a different behavior can be tentatively ascribed to the absence of π–π interactions between either styrene (or the conjugated ligand framework in $\mathbf{1}_{Ln}$) and the reagent. Indeed, such supramolecular interactions can be likely invoked to justify the excellent hydrothiolation performance measured with aromatic PhSH compared to the total absence of reactivity in the presence of the aliphatic counterparts (*i.e.* CySH). On this basis, it seems reasonable to postulate the existence of similar interactions to justify the performance of $\mathbf{1}_{Ln}$ in all other hydroelementation processes carried out with aromatic reagents.

Tandem catalytic CO_2 hydrosilylation to methane (CH_4) with $\mathbf{1}_{Sc}$* and $\mathbf{1}_{Y}$*

The deoxygenative CO_2 reduction to CH_4 in the presence of hydrosilanes is known to proceed through two successive (tandem) catalytic cycles where the initial CO_2 activation at the electrophilic metal ion of the cationized catalyst is supposed to initiate the process (Scheme 3). $B(C_6F_5)_3$ is well-known to activate hydrosilanes for the carbonyl[89,90] and carboxyl[90] reduction as well as for the cleavage of aryl and alkyl ethers[91] but the higher thermodynamic stability of CO_2 and its subsequent chemical inertness make mandatory the carbon dioxide preactivation at an electrophilic metal ion (Scheme 3, A) thus allowing the first kinetically sluggish hydrosilylation step to

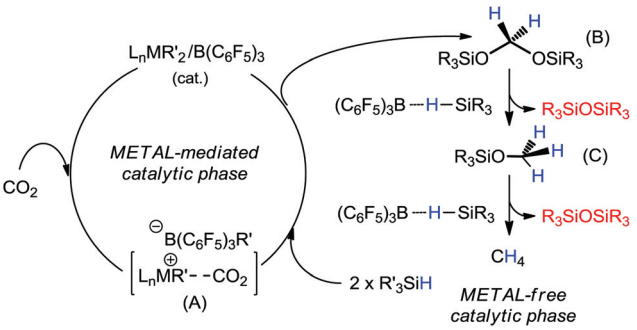

Scheme 3 Proposed mechanistic scheme for the *tandem* CO_2 hydrosilylation catalysis using a model R_3SiH hydrosylane as reductant and the Lewis acid $B(C_6F_5)_3$ as catalyst and hydrosilanes activator.

occur.[72,78] A metal-silylformate intermediate (not shown in the scheme) is supposed to undergo an additional hydrosilylation step to give the silylacetal species (B) that formally closes the cycle of metal-mediated transformations.[92–94] Afterwards, the borane–silane pair allows the process to be completed as a metal-free process till CH_4 production (Scheme 3).

Overall, the strong Lewis acid $B(C_6F_5)_3$ acts as an activator for the cationization of the bis(alkyl) catalyst precursor and activates the silane in the hydrosilylation steps.[72,78] The isolation and quantification of siloxane by-products is conventionally used to evaluate the catalyst performance.

Preliminary and qualitative catalytic hydrosilylation runs were carried out in a J Young NMR tube where a benzene-d_6 mixture of $\mathbf{1_Y}$ and $B(C_6F_5)_3$ (1 : 1.5 eq. with $PhMe_2SiH$; 1 : 1.1 eq. with $PhSiH_3$) was treated with various hydrosilanes before being pressurized with isotopically enriched $^{13}CO_2$ (99 atom% ^{13}C, 1 atm). All catalytic trials were systematically monitored by ^1H, $^{13}C\{^1H\}$ and ^{13}C NMR spectroscopy mainly with respect to distinctive signals attributed to CO_2, CH_4 and possible intermediates of the tandem hydrosilylation process. The $B(C_6F_5)_3$ addition to a solution of $\mathbf{1_Y}$ let to the almost immediate formation of a semisolid, not crystalline precipitate along with a solution color change from deep violet to dark brown. If the generation of a solid precipitate was somehow indicative of the occurred complex cationization, all our attempts to characterize the activated complex $\mathbf{1_Y}$* failed.[95] Indeed, ^1H and $^{13}C\{^1H\}$ NMR spectra recorded on $\mathbf{1_Y}$* gave only broad and undistinctive signals not suitable for a complete sample characterization. Furthermore, the activation of $\mathbf{1_Y}$ in more polar deuterated solvents resulted in the complete material decomposition with the rapid formation of intractable sticky solids.[95] Finally, the addition of a silane to $\mathbf{1_Y}$* did not change the solution/suspension color or the semisolid nature of the precipitate. Indeed, the ^1H NMR spectrum of each $\mathbf{1_Y}$*/silane mixture (recorded prior to its pressurization with $^{13}CO_2$) showed all distinctive and sharp signals of the unreacted silane as the background of a noisy sample baseline. The final $\mathbf{1_Y}$*/silane mixture pressurization step with $^{13}CO_2$ (1 atm) was found to trigger almost immediately the hydrosilylation process. When $PhMe_2SiH$ was selected as reducing agent, $\mathbf{1_Y}$* catalysed the complete $^{13}CO_2$ deoxygenative hydrosilylation to CH_4 in about 6 h along with the stoichiometric formation of the dimethylphenyl silylether $[Ph(CH_3)_2Si]_2O$ as the unique reaction side-product. The reaction course was systematically monitored by ^1H and $^{13}C\{^1H\}$ NMR spectroscopy till the complete $^{13}CO_2$ consumption. As Fig. 4A shows, the ^1H NMR spectra recorded at different reaction times indicate a progressive disappearance of the silane resonances along with the grow up of new high-field and distinctive signals attributed to $^{13}CH_4$ (δ_H = 0.16 ppm, d, $^1J_{HC}$ = 125 Hz) and dimethylphenyl silylether (δ_H = 0.32 ppm, s) as hydrosilylation by-product, respectively. The $^{13}CH_4$ formation was also followed by $^{13}C\{^1H\}$ NMR and ^{13}C NMR spectroscopy till the complete disappearance of the $^{13}CO_2$ singlet at 124.5 ppm (Fig. 4B).

In addition, the formation of $^{13}CH_4$ was double checked by the appearance of two sharp singlets at δ = −4.29 and 1.02 ppm whose attribution to methane and dimethylphenyl silylether, respectively, was unambiguously done on the basis of literature precedents. An additional proof of evidence for the above given peak assignment finally come from the distinctive ^1H coupled ^{13}C NMR patterns of both signals: $^{13}CH_4$ (δ = −4.29 ppm, quint, $^1J_{HC}$ = 125 Hz) and $[Ph(CH_3)_2Si]_2O$ (δ = 1.02 ppm, quart, $^1J_{HC}$ = 117 Hz) (green insets).

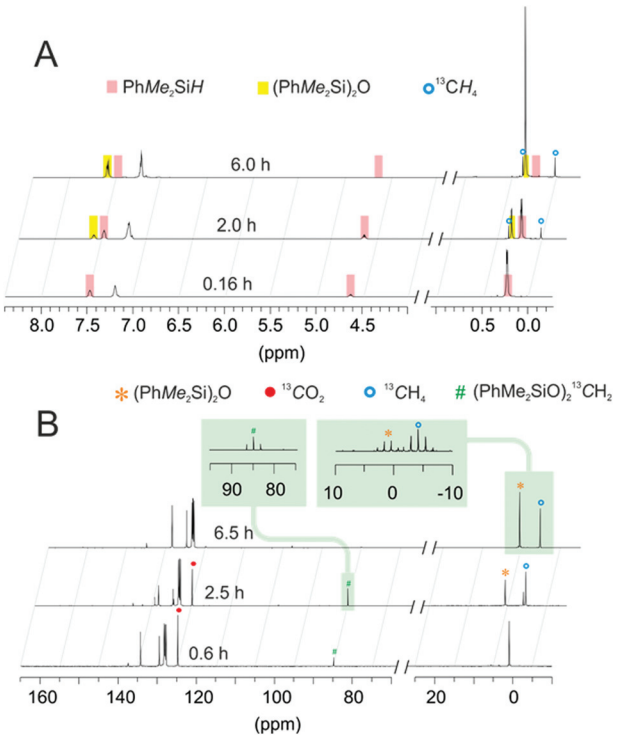

Fig. 4 ^1H and $^{13}C\{^1H\}$ NMR spectra (400 MHz, C_6D_6, 298 K) recorded at variable time for the $^{13}CO_2$ hydrosilylation reaction, using $Ph(CH_3)_2SiH$ as reductant. Conditions: r.t., $\mathbf{1_Y}$* (6 μmol, 1.2 mol%); (Y/B = 1/1.5). Green insets refer to ^{13}C NMR spectra.

A careful analysis of $^{13}C\{^1H\}$ and ^{13}C NMR spectra recorded at different reaction times have also shown the appearance of a new signal at δ = 84.9 ppm (t, $^1J_{CH}$ = 162.0 Hz, $^{13}CH_2$) that was ascribed to the transient formation of the bis(silyl) acetal $(PhMe_2SiO)_2$ $^{13}CH_2$ intermediate (Fig. 4B). A similar reaction scheme was followed in the case of $PhSiH_3$ as reducing agent. According to other literature precedents, the reaction kinetics was markedly affected by the choice of the hydrosilanes used. As a result, in the case of $PhSiH_3$ an almost complete $^{13}CO_2$ consumption was observed for prolonged reaction times only (>90 h). For the present issue, the reaction path was even easier to be followed by $^{13}C\{^1H\}$ NMR spectroscopy as CH_4 was the unique reaction product. No other appreciable silane signals were observed spectroscopically. Indeed, $PhSiH_3$ hydrosilylation was expected to give silsesquioxane polymers of general formula $(PhSiO_{1.5})_n$ as unique silane by-products (Fig. S10†). All these data taken together provided evidence of the ability of the organolanthanides from this series to catalyze the tandem hydrosilylation reaction.

To complete the study and to provide a more accurate and quantitative analysis of the reaction products and the catalysts turnover, $\mathbf{1_Y}$ and $\mathbf{1_{Sc}}$ were scrutinized as precursors for the tandem hydrosilylation in a batch reactor using various hydrosilanes as reducing agents. To this aim, a Teflon-lined 20 mL stainless-steel reactor, equipped with a magnetic stirrer bar, was charged with a toluene solution of the pre-catalyst under inert atmosphere, hence $B(C_6F_5)_3$ and a selected silane (**A**, **B** or **C**, see Table 4) were added in sequence prior to the reactor pressurization with CO_2 (1 atm at room temperature). Afterwards, all crude reaction mixtures were sampled and analysed *via* GC-MS before removing all solvents and volatiles under vacuum. Except for reactions with $PhSiH_3$ (**B**) as reducing agent, all other dried mixtures obtained upon reaction with hydrosilanes **A** and **C** were monitored *via* ^{1}H NMR spectroscopy as to provide the molar fraction of each silane product or intermediate generated throughout the catalytic run. Catalysts turnover number (TON) and turnover frequency (TOF) were finally determined from the weight of isolated siloxanes (or silsesquioxane polymers in the case of **B** as reductant) and values were expressed as Si–H bonds reacted per mmol of catalyst (TON) per hour (TOF). Table 4, lists all main catalytic outcomes recorded in the reduction process with both activated organolanthanides in the presence of various hydrosilanes. With $Ph(CH_3)_2SiH$ (**A**), $\mathbf{1_Y}$* showed higher performance compared to its scandium ($\mathbf{1_{Sc}}$*) counterpart with a TOF value of 26 and a calculated methane yield as high as 66% (Table 4, entries 1 *vs.* 2). In the case of $\mathbf{1_Y}$*, we have also observed an almost complete dimethyl–phenyl silane (4.1 eq. *vs.* CO_2) consumption (<3% residue) after 8 h. Nevertheless, the reaction course was incomplete as a 66 : 34 mixture of $(PhMe_2Si)_2O$ and the intermediate $(PhMe_2SiO)_2CH_2$, respectively, was obtained after the reaction work-up. Noteworthy, when the same reaction was carried out in the presence of a borane excess (Y : B = 1 : 1.5 instead of 1 : 1.1), $(PhMe_2Si)_2O$ was the only silane side-product (>95 mol% of the staring **A**) isolated already after 4 h. Under these optimized conditions, catalyst TOF was nearly doubled (Table 4, entries 3 *vs.* 1). Overall, it can be inferred that a large excess of borane in the mixture had beneficial effects on the hydrosilylation kinetics. If $\mathbf{1_Y}$* was formed almost immediately and quantitatively upon the treatment of its neutral counterpart with 1.1 eq. of $B(C_6F_5)_3$ (as witnessed by the rapid precipitation of $\mathbf{1_Y}$* and disappearance of distinctive ^{1}H NMR signals of $\mathbf{1_Y}$ from the reaction mixture), the excess of borane was found to foster the silane activation and reduction kinetics of the last metal-free hydrosilylation steps mainly [from the bis(silyl)acetal intermediate (B) to methane *via* a methoxy–silane intermediate (C), see Scheme 3]. When $PhSiH_3$ (**B**) was employed as hydrosilylating agent (1.35 eq. *vs.* CO_2), $\mathbf{1_{Sc}}$* showed slightly better catalytic performance of its $\mathbf{1_Y}$* counterpart (Table 4, entries 6 *vs.* 5) under identical conditions (Ln : B = 1 : 1.1). Anyway, the catalytic outcomes recorded with **B** as reductant were in line with the more sluggish kinetics already observed in J Young NMR tube experiments using isotopically enriched $^{13}CO_2$.

Hence, catalysts' TOFs resulted markedly lower compared to those obtained with silane **A** (Table 4, entries 5 *vs.* 1 and 6 *vs.* 2). Finally, Et_2MeSiH (**C**) was selected as a more sterically demanding reducing agent [compared to $Ph(CH_3)_2SiH$] with the final aim at studying the $\mathbf{1_{Ln}}$* sensitivity to the hindrance around the Si–H bond. As Table 4, entry 7 shows, after 40 h reaction with $\mathbf{1_Y}$*, only 31 mol% of Et_2MeSiH were reacted of which more than 90% to give the $(Et_2MeSiO)_2CH_2$ intermediate. With $\mathbf{1_{Sc}}$* the mol of Si–H bonds reacted were even lower (24 mol% after 40 h; Table 4, entry 8) although the % of $(Et_2MeSi)_2O$ in the mixture (hence CH_4 produced) was slightly

Table 4 CO_2 hydrosilylation by $\mathbf{1_Y}$* and $\mathbf{1_{Sc}}$* [a]

Entry	Cat. $\mathbf{1_{Ln}}$/B	Silane[b]	Time (h)	Si-Byproducts	mmol[c]	TON[d]	TOF[e]	CH_4 [f] yield (%)
1	$\mathbf{1_Y}$*	A	8	$(PhMe_2Si)_2O$	2.18	207	26	65.7
				$(PhMe_2SiO)_2CH_2$	1.13			—
2	$\mathbf{1_{Sc}}$*	A	8	$(PhMe_2Si)_2O$	1.30	135	17	39.1
				$(PhMe_2SiO)_2CH_2$	0.86			—
3[g]	$\mathbf{1_Y}$*	A	4	$(PhMe_2Si)_2O$	3.24	202	50	97.5
4[g]	$\mathbf{1_{Sc}}$*	A	4	$(PhMe_2Si)_2O$	2.46	154	38	74.1
5	$\mathbf{1_Y}$*	B	72	$(PhSiO_{1.5})_n$	2.16	135	1.9	65.0
6	$\mathbf{1_{Sc}}$*	B	72	$(PhSiO_{1.5})_n$	3.24	202	2.8	97.6
7	$\mathbf{1_Y}$*	C	40	$(Et_2MeSi)_2O$	0.10	66	1.6	3.1
				$(Et_2MeSiO)_2CH_2$	0.95			—
8	$\mathbf{1_{Sc}}$*	C	40	$(Et_2MeSi)_2O$	0.14	51	1.3	4.1
				$(Et_2MeSiO)_2CH_2$	0.68			—
9[g]	$\mathbf{1_Y}$*	C	40	$(Et_2MeSi)_2O$	2.56	182	4.5	77.3
				$(Et_2MeSiO)_2CH_2$	0.35			—
10[g]	$\mathbf{1_{Sc}}$*	C	40	$(Et_2MeSi)_2O$	2.30	176	4.4	69.3
				$(Et_2MeSiO)_2CH_2$	0.52			—

[a] Reaction conditions: Catalyst precursor (16 μmol, 0.44 mol% per Si–H bond), $B(C_6F_5)_3$ (17.6 μmol, M/B = 1/1.1, 0.48 mol% per Si–H bond), CO_2 (1 atm, 295 K, 20 mL, 0.83 mmol), toluene (2.5 mL), 295 K. [b] Silanes: (**A**) $PhMe_2SiH$ (3.40 mmol); (**B**) $PhSiH_3$ (1.12 mmol); (**C**) Et_2MeSiH (3.40 mmol). [c] mmol of silane side-products given as mmol of reacted Si–H bond. In case of mixtures, the relative molar fractions have been determined from by ^{1}H NMR spectra recorded on the crude mixture after evaporation of all solvents and volatiles and bulb-to-bulb distillation/purification. [d] TON calculated on the basis of Si–H reacted per mmol of catalyst. [e] TOF calculated as TON h^{-1}. [f] Calculated as: [(mmol of reacted silane/4)/(mmol of CO_2)] × 100. [g] With 24 μmol of $B(C_6F_5)_3$ (M/B = 1/1.5, 0.70 mol% per Si–H bond).

higher (17%) compared to the yttrium-catalyzed reaction. As for the case of reductant **A**, also with **C** the use of an excess of $B(C_6F_5)_3$ had beneficial effects on the catalysts performance. Indeed, when a Ln : B ratio increased from 1 : 1.1 to 1 : 1.5, methane production (% yield) grow up remarkably, irrespective to the nature of the activated organolanthanide complex at work (Table 4, entries 10 *vs*. 8 and 9 *vs*. 7). Overall, more sterically crowded Si–H bonds translated into sluggish process rates and catalytic performance very close each other, regardless of the nature of the metal ion employed in the process. At the same time, the use of a larger borane excess triggered positively both the rate of the metal-assisted and metal-free reduction steps in the tandem hydrosilylation process. In spite of the general process feasibility, the best catalytic performance obtained with $\mathbf{1_{Ln}}$* in the tandem CO_2 hydrosilylation reaction is appreciably lower than that of the benchmark $\kappa^3\{\mathcal{N}^-,N,\mathcal{N}^-\}M^{IV}(CH_2Ph)_2/B(C_6F_5)_3$ (M^{IV} = Zr, Hf) system under the same hydrosilylation conditions and whatever the nature of the hydrosilylating reagents used.[78]

Conclusions

In conclusion, a new class of bis(alkyl) Sc and Y complexes $[N,N^{py},N^-]Ln(CH_2SiMe_3)_2(THF)_n$ coordinated by a tridentate monoanionic amidopyridinate ligand have been synthesised and completely characterized. At odds with bis(alkyl) species previously reported by some of us and containing benzothiazolyl substituted amidopyridinate frameworks,[79] $[N,N^{py},N^-]Ln(CH_2SiMe_3)_2(THF)_n$ systems from this series with a N-protected imidazolate group proved to be robust and thermally stable compounds. They do not undergo intramolecular rearrangements through heteroaromatic ring opening paths. The organolanthanides were finally scrutinized as catalysts or catalyst precursors in a relatively wide variety of challenging catalytic transformations. Indeed, they have successfully been employed as either effective polymerization pre-catalysts for the *cis*-1,4 stereo-enriched polyisoprene (PIP) production as well as good catalyst candidates for the anti-Markovnikov intermolecular addition of a variety of E–H containing molecules (E = N, S, P) to a model unsaturated C=C bond substrate. Finally, selected rare-earth compounds from this series have also been investigated as valuable catalyst precursors for the tandem CO_2 hydrosilylation to CH_4 in the presence of a series of organosilanes as reducing agents ($PhMe_2SiH$, $PhSiH_3$, Et_2MeSiH) and the strong Lewis acid $B(C_6F_5)_3$ as catalyst and silane(s)-activator. Overall, these catalytic outcomes highlight the high versatility of bis(alkyl)organolanthanides in catalysis and open new horizons for their future exploitation in processes at the heart of renewable energy technology.

Experimental section

General details and considerations

All air- and/or moisture-sensitive reactions were performed under inert atmosphere using standard Schlenk-type vessels or in a dry-box filled with nitrogen. THF, toluene and hexane were purified by distillation from sodium/triglyme benzophenone ketyl and stored over CaH_2. Benzene-d_6 was dried over sodium/benzophenone ketyl and condensed *in vacuo* prior to use. Tris(alkyl) precursors $Ln(CH_2SiMe_3)_3(THF)_2$[96] and the ligand $[N,N^{py},N^-]H$ (**1**) were prepared according to previously published procedures. $PhMe_2SiH$, Ph_3SiH and Et_2MeSiH were purchased from Aldrich Chemical Co. Inc. and used as received. $[Ph_3C][B(C_6F_5)_4]$ and $[HNMe_2Ph][B(C_6F_5)_4]$ were obtained from Synor Ltd, while tris-(pentafluorophenyl)borane $[B(C_6F_5)_3]$ was obtained from Strem Chemicals Inc. and it was sublimed at 70 °C under (static) high reduced pressure prior to be used in catalysis. ^1H and $^{13}C\{^1H\}$ and 2D (COSY H,H; HETCOR H,C) NMR spectra were recorded on a Bruker Avance III-400 spectrometer (400.13 and 100.61 MHz for ^1H and ^{13}C, respectively). Chemical shifts are reported in ppm relative to TMS and peaks are referenced to the chemical shifts of residual solvent resonances (^1H and ^{13}C). The C, H, N elemental analyses are conducted in the microanalytical laboratory of IMOC. Lanthanide metal analysis was carried out by complexometric titration.[97]

Synthesis of $\mathbf{1_{Sc}}$. A solution of **1** (0.108 g; 0.39 mmol) in toluene (10 mL) was added at 0 °C to a solution of Sc $(CH_2SiMe_3)_3(THF)_2$ (0.176 g; 0.39 mmol) in toluene (5 mL). The reaction mixture was stirred at 0 °C for 1 h and was allowed to warm to room temperature, the volatiles were removed in vacuum. The crude products were re-dissolved in fresh toluene (5 mL) and stored at −30 °C for 48 h till the formation of the dark red microcrystals of $\mathbf{1_{Sc}}$. The mother liquor was decanted from the product, the crystals were washed with cold toluene and dried in vacuum for 10 min. Dark red crystals of complex $\mathbf{1_{Sc}}$ were isolated in 83% yield (0.244 g). ^1H NMR (400 MHz, C_6D_6, 293 K): 0.01 (s, 18H, $CH_2Si(CH_3)_3$), 0.31 (d, $^2J_{HH}$ = 11.3 Hz, 2H, CH_2SiMe_3), 0.65 (d, $^2J_{HH}$ = 11.3 Hz, 2H, CH_2SiMe_3), 0.83 (t, $^3J_{HH}$ = 7.0 Hz, 3H, CH_3CH_2O), 1.43 (d, $^3J_{HH}$ = 6.9 Hz, 6H, $CH(CH_3)_2$), 1.71 (d, $^3J_{HH}$ = 6.9 Hz, 6H, $CH(CH_3)_2$), 3.05 (q, $^3J_{HH}$ = 7.0 Hz, 2H, CH_3CH_2O), 4.34 (sept, $^3J_{HH}$ = 6.9 Hz, 2H, $CH(CH_3)_2$), 4.82 (s, 2H, CH_2OEt), 4.92 (s, 2H, CH_2NAr), 6.43 (d, $^3J_{HH}$ = 8.0 Hz, 1H, C*H* Ar), 6.82 (t, $^3J_{HH}$ = 7.9 Hz, 1H, C*H* Ar), 6.88 (d, $^3J_{HH}$ = 8.3 Hz, 1H, C*H* Ar), 7.09 (m, 1H, C*H* Ar, overlaps with solvate toluene), 7.25 (t, $^3J_{HH}$ = 7.8 Hz, 1H, C*H* Ar), 7.36 (dd, $^3J_{HH}$ = 8.7 Hz, $^3J_{HH}$ = 6.2 Hz, 1H, C*H* Ar), 7.42 (m, 2H, C*H* Ar), 7.54 (d, $^3J_{HH}$ = 7.7 Hz, 1H, C*H* Ar), 8.71 (d, $^3J_{HH}$ = 8.2 Hz, 1H, C*H* Ar) ppm. $^{13}C\{^1H\}$ NMR (100 MHz, C_6D_6, 293 K): 3.6 (s, $CH_2Si(CH_3)_3$), 14.7 (s, CH_3CH_2O), 24.7 (s, $CH(CH_3)_2$), 27.8 (s, $CH(CH_3)_2$), 28.0 (s, $CH(CH_3)_2$), 39.1 (br s, $ScCH_2SiMe_3$), 65.0 (s, CH_2NAr), 65.4 (s, CH_3CH_2O), 73.1 (s, CH_2OEt), 109.6 (s, C*H* Ar), 119.4 (s, C*H* Ar), 121.5 (s, C*H* Ar), 123.5 (s, C*H* Ar), 124.4 (s, C*H* Ar), 124.7 (s, C*H* Ar), 125.8 (s, C*H* Ar), 126.0 (s, C*H* Ar), 136.3 (s, C Ar), 137.9 (s, C Ar), 139.7 (s, CH Ar), 143.2 (s, C Ar), 146.8 (s, C Ar), 150.8 (s, C Ar), 152.0 (s, C Ar), 168.8 (s, C Ar) ppm. Elemental analysis calculated for $C_{36}H_{55}N_4OScSi_2\cdot(C_7H_8)$ (753.11 g mol^{-1}): C, 68.58; H, 8.43; N, 7.44; Sc, 5.97. Found: C 68.75, H 8.67, N 7.22, Sc 5.71.

Synthesis of $\mathbf{1_Y}$. A solution of **1** (0.235 g; 0.54 mmol) in toluene (10 mL) was added to a solution of

$Y(CH_2SiMe_3)_3(THF)_2$ (0.265 g; 0.54 mmol) in toluene (10 mL) at 0 °C. The reaction mixture was stirred for 1 h and was allowed to warm to room temperature. The volatiles were removed in vacuum and the crude products were re-dissolved in fresh toluene (10 mL) and stored at −20 °C for 48 h till the formation of dark red crystals. The mother liquor was decanted, the product was washed with cold toluene and dried in vacuum for 10 min. Dark red crystals of complex $\mathbf{1_Y}$ were isolated in 79% yield (0.337 g). ^{1}H NMR (400 MHz, C_6D_6, 293 K): −0.10 (dd, $^2J_{HH}$ = 10.7 Hz, $^2J_{YH}$ = 2.3 Hz, 2H, CH_2SiMe$_3$), 0.07 (s, 18H, $CH_2Si(CH_3)_3$), 0.13 (br d, $^2J_{HH}$ = 10.7 Hz, YH splitting not observed, 2H, CH_2SiMe$_3$), 0.82 (t, $^3J_{HH}$ = 6.8 Hz, 3H, CH_3CH$_2$O), 1.44 (d, $^3J_{HH}$ = 6.6 Hz, 6H, CH(CH_3)$_2$), 1.68 (d, $^3J_{HH}$ = 6.6 Hz, 6H, CH(CH_3)$_2$), 3.03 (q, $^3J_{HH}$ = 6.8 Hz, 2H, CH$_3$CH_2O), 4.28 (sept, $^3J_{HH}$ = 6.6 Hz, 2H, CH(CH$_3$)$_2$), 4.78 (s, 2H, CH_2OEt), 4.97 (s, 2H, CH_2NAr), 6.49 (d, $^3J_{HH}$ = 7.5 Hz, 1H, CH Ar), 6.84 (m, 2H, CH Ar), 7.16 (m, 1H, CH Ar overlaps with C_6D_6), 7.20 (t, $^3J_{HH}$ = 7.6 Hz, 1H, CH Ar), 7.32 (d, $^3J_{HH}$ = 8.1 Hz, 1H, CH Ar), 7.39 (d, $^3J_{HH}$ = 7.2 Hz, 2H, CH Ar), 7.62 (d, $^3J_{HH}$ = 7.3 Hz, 1H, CH Ar), 8.56 (d, $^3J_{HH}$ = 8.1 Hz, 1H, CH Ar) ppm. ^{13}C{^{1}H} NMR (100 MHz, C_6D_6, 293 K): 3.7 (s, $CH_2Si(CH_3)_3$), 14.4 (s, CH_3CH_2O), 24.8 (s, CH(CH_3)$_2$), 27.4 (s, CH(CH_3)$_2$), 27.7 (s, CH(CH$_3$)$_2$), 34.0 (d, $^1J_{YC}$ = 38.5 Hz, CH_2SiMe$_3$), 65.1 (s, CH$_3$CH_2O), 65.5 (d, $^1J_{YC}$ = 2.5 Hz, CH_2NAr), 72.9 (s, CH_2OEt), 109.5 (s, CH Ar), 119.7 (s, CH Ar), 120.6 (s, CH Ar), 123.6 (s, CH Ar), 123.9 (s, CH Ar), 124.0 (s, CH Ar), 125.6 (s, CH Ar), 125.8 (s, CH Ar), 135.8 (s, C Ar), 138.2 (s, CH Ar), 139.3 (s, C Ar), 143.2 (s, C Ar), 146.8 (s, C Ar), 149.6 (s, C Ar), 152.6 (s, C Ar), 169.4 (s, C Ar) ppm. The 2D Y–H g-HMQC NMR spectrum was set with hsqcetgp pulse program, delay $D1$ = 1.5 s, cnst2 = 200, GPZ2 = 14% (400; 19.6 MHz, C_6D_6, 293 K): −0.11; 1033 (Y-CH_2SiMe$_3$), 0.06; 1033 (Y-CH_2Si(CH_3)$_3$), 0.13; 1033 (Y-CH_2SiMe$_3$), 4.97; 1033 (Y-NCH_2Ar) ppm. Elemental analysis calculated for $C_{36}H_{55}N_4OSi_2Y\cdot(C_7H_8)$ (797.06 g mol^{-1}): C, 64.80; H, 7.97; N, 7.03; Y, 11.15. Found: C 64.95, H 8.13, N 7.09, Y 10.93.

Synthesis of $\mathbf{1_Y^{THF}}$. A solution of **1** (0.205 g; 0.46 mmol) in hexane (15 mL) was added to a solution of $Y(CH_2SiMe_3)_3(THF)_2$ (0.230 g; 0.46 mmol) in hexane (15 mL) at 0 °C. The reaction mixture was stirred for 1 h, then it was allowed to warm to room temperature and the volatiles were removed in vacuum. The crude products were re-dissolved in hexane/THF mixture (4/1, 10 mL) and the solution was stored at −30 °C for 12 h. The mother liquor was decanted and the crystals were washed with cold hexane and dried in vacuum for 10 min. Dark red crystals of complex $\mathbf{1_Y^{THF}}$ were isolated in 74% yield (0.267 g; 0.34 mmol). ^{1}H NMR (400 MHz, C_6D_6, 293 K): −0.68 (dd, $^2J_{HH}$ = 10.7 Hz, $^2J_{YH}$ = 2.0 Hz, 2H, CH_2SiMe_3), −0.60 (dd, $^2J_{HH}$ = 10.7 Hz, $^2J_{YH}$ = 2.8 Hz, 2H, CH_2SiMe$_3$), −0.25 (s, 18H, $CH_2Si(CH_3)_3$), 0.90 (t, $^3J_{HH}$ = 6.9 Hz, 3H, CH_3CH$_2$O), 1.35 (br s, 4H, β-CH_2, THF), 1.47 (d, $^3J_{HH}$ = 6.8 Hz, 6H, CH(CH_3)$_2$), 1.56 (d, $^3J_{HH}$ = 6.8 Hz, 6H, CH(CH_3)$_2$), 3.24 (q, $^3J_{HH}$ = 6.9 Hz, 2H, CH$_3$CH_2O), 3.55 (br. s, 4H, α-CH_2, THF), 4.33 (sept, $^3J_{HH}$ = 6.8 Hz, 2H, CH(CH$_3$)$_2$), 5.00 (s, 2H, CH_2NAr), 5.10 (s, 2H, CH_2OEt), 6.58 (d, $^3J_{HH}$ = 7.9 Hz, 1H, CH Ar), 7.00 (m, 2H, CH Ar), 7.23 (m, 2H, CH Ar), 7.31 (m, 3H, CH Ar), 7.99 (d, $^3J_{HH}$ = 7.8 Hz, 1H, CH Ar), 8.21 (d, $^3J_{HH}$ = 8.0 Hz, 1H, CH Ar) ppm. ^{13}C{^{1}H} NMR (100 MHz, C_6D_6, 293 K): 3.9 (s, $CH_2Si(CH_3)_3$), 14.4 (s, CH_3CH_2O), 24.9 (s, CH(CH_3)$_2$), 25.3 (br s, β-CH_2, THF), 26.7 (br d, $^1J_{YC}$ = 33.7 Hz, YCH_2SiMe$_3$), 27.2 (s, CH(CH$_3$)$_2$), 27.3 (s, CH(CH_3)$_2$), 64.9 (s, CH_3CH_2O), 66.0 (d, $^2J_{YC}$ = 2.5 Hz, CH_2NAr), 68.1 (br s, α-CH_2, THF), 72.8 (s, OCH_2N), 109.6 (s, CH Ar), 120.6 (s, CH Ar), 123.3 (s, CH Ar), 123.6 (s, CH Ar), 123.8 (s, CH Ar), 124.7 (s, CH Ar), 125.3 (s, CH Ar), 125.4 (s, CH Ar), 136.4 (s, C Ar), 137.9 (s, CH Ar), 144.1 (s, C Ar), 147.2 (s, C Ar) 150.9 (s, C Ar), 151.3 (s, C Ar), 169.3 (s, C Ar) ppm. The 2D Y–H g-HMQC NMR spectrum was set with hsqcetgp pulse program, delay $D1$ = 1.5 s, cnst2 = 200, GPZ2 = 14% (400; 19.6 MHz, 293 K, C_6D_6): −0.68; 800.9 (Y-CH_2SiMe$_3$), −0.60; 801 (Y-CH_2SiMe3), −0.25; 801 (Y-CH_2Si(CH_3)$_3$), 5.00; 801 (Y-NCH_2Pyr) ppm. Elemental analysis calculated for $C_{40}H_{63}N_4O_2Si_2Y$ (777.03 g mol^{-1}): C 61.83, H 8.17, N 7.21, Y 11.44. Found: C 62.13, H 8.09, N 7.38, Y 11.23.

Polymerization of isoprene

All polymerization tests were conducted under a nitrogen atmosphere. In a typical procedure, 10 μmol of the selected catalyst precursor ($\mathbf{1_{Sc}}$, $\mathbf{1_Y}$ and $\mathbf{1_Y^{THF}}$) was dissolved in toluene (3 mL) and treated with a solution of the proper activator {10 μmol; $[CPh_3][B(C_6F_5)_4]$ or $[HNMe_2Ph][B(C_6F_5)_4]$} in toluene (2 mL). 10 equiv. of Al^{i}Bu$_3$ (0.1 mL, 100 μmol, 1.0 M in toluene) were added and the reaction mixture was stirred for 2 min; then 1 mL (10 mmol) of isoprene was added *via* syringe at room temperature. The reaction mixture was stirred for 2–18 h. Afterwards, polymerization was stopped by quenching the mixture with an excess of methanol (20 mL) and dried under vacuum at ambient temperature to a constant weight. The polymer microstructures were determined by ^{1}H and ^{13}C{^{1}H} NMR spectroscopy in $CDCl_3$ at r.t. GPC of polyisoprenes was performed in THF at 20 °C. The average molecular masses (M_n) and polydispersity (M_w/M_n) of the polymers were calculated with reference to a universal calibration against polysterene standards.

General procedure for hydroelementation reactions

In typical hydrophosphination, hydroamination or hydrothiolation experiments, the complexes $\mathbf{1_{Sc}}$, $\mathbf{1_Y}$ and $\mathbf{1_Y^{THF}}$ (10 μmol) were loaded in tube in the glovebox, then at first styrene (0.5 mmol; 50 equiv.) was added at ambient temperature and then E–H substrate was added (0.5 mmol, 50 equiv.). The reaction mixture was heated at 70 °C for a definite time in a pre-heated oil bath. After the desired reaction time, $CDCl_3$ was added to the reaction mixture, and the ^{1}H and ^{31}P{^{1}H} (for hydrophosphination) or ^{13}C{^{1}H} (for hydroamination and hydrothiolation) NMR spectra were recorded. Conversion was determined by integrating the remaining substrates and the newly formed addition product in the ^{1}H spectra as well as the remaining and newly formed phosphines in the ^{31}P{^{1}H}.

General procedure for NMR tube scale reduction of isotopically enriched $^{13}CO_2$ with hydrosilanes catalyzed by $\mathbf{1_Y/B(C_6F_5)_3}$

A 3 mL J Young NMR tube was charged under nitrogen atmosphere with a pre-catalyst solution of $\mathbf{1_Y}$ (6.0 μmol, in C_6D_6

0.4 mL; 1.2 mol% *vs*. $PhMe_2SiH$ or 1.5 mol% *vs*. $PhSiH_3$). Afterwards, a solution of $B(C_6F_5)_3$ (9 μmol or 6.6 μmol) in dry and degassed C_6D_6 (0.4 mL) and the proper hydrosilane (4.08 eq. of $PhMe_2SiH$ *vs*. $^{13}CO_2$; 1.35 eq. of $PhSiH_3$ *vs*. $^{13}CO_2$) were rapidly added in sequence. The tube underwent three successive evacuation/refilling cycles with $^{13}CO_2$ and it was finally charged with a positive $^{13}CO_2$ pressure of 1 atm (*ca.* 124 μmol). The reaction course was followed *via* ^1H, ^{13}C and $^{13}C\{^1H\}$ NMR at variable times.

General procedure for the reduction of CO_2 with hydrosilane catalyzed by $\mathbf{1_{Sc}}(\mathbf{1_Y})/B(C_6F_5)_3$

A 20 mL stainless-steel reactor, equipped with a magnetic stirrer bar, was charged under an inert atmosphere with a toluene solution of the precatalyst ($\mathbf{1_{Sc}}$ or $\mathbf{1_Y}$) in dry and degassed toluene (1.5 mL). The reactor was sealed, then $B(C_6F_5)_3$ (1.1 or 1.5 equiv. with respect to the metal in 1 mL of toluene) and neat hydrosilane (3.40 mmol for **A** and **C** or 1.13 mmol for **B**) were added by syringe in sequence. The system was submitted immediately to successive evacuation/refilling cycles (three cycles) with CO_2 before it was charged with a positive pressure of CO_2 (1 atm, 20 mL, 0.83 mmol). After the first addition (precatalyst), the mixture was maintained under stirring for 2 min before it was treated with the hydrosilane. The final mixture was then maintained under stirring at RT for the desired time. Afterwards, the reactor was opened and its contents were transferred into a glass flask before all volatiles were removed under reduced pressure. The composition of each crude mixture and relative molar fractions of all compounds were followed by using GC-MS and ^1H NMR analysis. After solvent removal, all crude residues from reactions with hydrosilanes **A** and **C** were distilled by using a bulb-to-bulb distillation system (Kugelrohr) to give $(R_3SiO)_2CH_2$ and/or $(R_3Si)_2O$ as inseparable colorless oils that were analyzed by using ^1H NMR spectroscopy in C_6D_6. For the reactions with $PhSiH_3$ (**B**) solvent evaporation gave organosilicon compounds of the general formula $(PhSiO_{1.5})_n$ as an offwhite viscous oil that was washed thoroughly with pentane and dried under vacuum to constant weight. The TON and TOF were measured experimentally from the isolated Si byproducts (siloxanes) and expressed conventionally as Si–H bonds reacted per mmol of catalyst (TON) per hour (TOF).

X-Ray crystallography

The X-ray data for $\mathbf{1_{Sc}}$, $\mathbf{1_Y}$ and $\mathbf{1_Y^{THF}}$ were collected on Bruker Apex II ($\mathbf{1_{Sc}}$, $\mathbf{1_Y^{THF}}$; T = 120 K) and Bruker Smart Apex ($\mathbf{1_Y}$; T = 100 K) diffractometers (MoKα-radiation, ω-scans technique, λ = 0.71073Å) using Smart and APEX2[98] software packages. The structures were solved by direct methods and were refined by full-matrix least squares on F^2 for all data using SHELX.[99] SADABS[100] was used to perform absorption corrections. All non-hydrogen atoms in $\mathbf{1_{Sc}}$, $\mathbf{1_Y}$ and $\mathbf{1_Y^{THF}}$ were found from Fourier syntheses of electron density and were refined anisotropically. All hydrogen atoms were placed in calculated positions and were refined in the "riding" model with $U(H)_{iso}$ = $1.2U_{eq}$ of their parent atoms ($U(H)_{iso}$ = $1.5U_{eq}$ for methyl groups). The crystallographic data and structures refinement details for $\mathbf{1_{Sc}}$, $\mathbf{1_Y}$ and $\mathbf{1_Y^{THF}}$ are given in Table S1 (ESI).† CCDC 1956756 ($\mathbf{1_{Sc}}$), 1956757 ($\mathbf{1_Y}$) and 1956758 ($\mathbf{1_Y^{THF}}$)† contains the supplementary crystallographic data for this paper.

Conflicts of interest

There are no conflicts to declare.

Acknowledgements

This work was financially supported by the Russian Science Foundation (grant 17-73-20262). The X-ray studies of $\mathbf{1_{Sc}}$, $\mathbf{1_Y}$ and $\mathbf{1_Y^{THF}}$ have been carried out in the framework of the Russian state assignment using the equipment of the Analytical Center of the G. A. Razuvaev Institute of Organometallic Chemistry, RAS. G. G. thanks the TRAINER project (Catalysts for Transition to Renewable Energy Future) of the "Make our Planet Great Again" program (Ref. ANR-17-MPGA-0017) for support. The Italian team would also like to thank the Italian MIUR through the PRIN 2017 Project Multi-e (20179337R7) "Multielectron transfer for the conversion of small molecules: an enabling technology for the chemical use of renewable energy" for financial support to this work.

Notes and references

1 M. Zimmermann and R. Anwander, *Chem. Rev.*, 2010, **110**, 6194–6259.
2 N. Marques, A. Sella and J. Takats, *Chem. Rev.*, 2002, **102**, 2137–2160.
3 S. A. Cotton, *Coord. Chem. Rev.*, 1997, **160**, 93–127.
4 W. E. Piers and D. J. H. Emslie, *Coord. Chem. Rev.*, 2002, **233–234**, 131–155.
5 A. A. Trifonov, *Russ. Chem. Rev.*, 2007, **76**, 1122–1144.
6 A. A. Trifonov and D. M. Lyubov, *Coord. Chem. Rev.*, 2017, **340**, 10–61.
7 A. A. Trifonov, *Coord. Chem. Rev.*, 2010, **254**, 1327–1347.
8 M. Nishiura and Z. Hou, *Nat. Chem.*, 2010, **2**, 257–268.
9 M. Nishiura, F. Guo and Z. Hou, *Acc. Chem. Res.*, 2015, **48**, 2209–2220.
10 P. L. Watson and G. W. Parshall, *Acc. Chem. Res.*, 1985, **18**, 51–56.
11 K. R. D. Johnson and P. G. Hayes, *Chem. Soc. Rev.*, 2013, **42**, 1947–1960.
12 H. Tsurugi, K. Yamamoto, H. Nagae, H. Kaneko and K. Mashima, *Dalton Trans.*, 2014, **43**, 2331–2343.
13 P. L. Arnold, M. W. McMullon, J. Rieb and F. E. Kühn, *Angew. Chem., Int. Ed.*, 2015, **54**, 82–100.
14 J. Oyamada, M. Nishiura and Z. Hou, *Angew. Chem., Int. Ed.*, 2011, **50**, 10720–10723.
15 A. G. Trambitas, T. K. Panda, J. Jenter, P. W. Roesky, C. Daniliuc, C. G. Hrib, P. G. Jones and M. Tamm, *Inorg. Chem.*, 2010, **49**, 2435–2446.

16 M. Ohashi, M. Konkol, I. Del Rosal, R. Poteau, L. Maron and J. Okuda, *J. Am. Chem. Soc.*, 2008, **130**, 6920–6921.
17 D. S. Levine, T. D. Tilley and R. A. Andersen, *Chem. Commun.*, 2017, **53**, 11881–11884.
18 S. Ge, A. Meetsma and B. Hessen, *Organometallics*, 2008, **27**, 3131–3135.
19 B. R. Elvidge, S. Arndt, T. P. Spaniol and J. Okuda, *Dalton Trans.*, 2006, **7**, 890–901.
20 G. A. Molander and J. A. C. Romero, *Chem. Rev.*, 2002, **102**, 2161–2186.
21 G. Zhan, H.-L. Teng, Y. Luo, S.-J. Lou, M. Nishiura and Z. Hou, *Angew. Chem., Int. Ed.*, 2018, **57**, 12342–12346.
22 X. Xu, Y. Chen, J. Feng, G. Zou and J. Sun, *Organometallics*, 2010, **29**, 549–553.
23 N. K. Hangaly, A. R. Petrov, K. A. Rufanov, K. Harms, M. Elfferding and J. Sundermeyer, *Organometallics*, 2011, **30**, 4544–4554.
24 S. Bambirra, H. Tsurugi, D. van Leusen and B. Hessen, *Dalton Trans.*, 2006, 1157–1161, DOI: 10.1039/B512135C.
25 T. E. Müller, K. C. Hultzsch, M. Yus, F. Foubelo and M. Tada, *Chem. Rev.*, 2008, **108**, 3795–3892.
26 J. Hannedouche, J. Collin, A. Trifonov and E. Schulz, *J. Organomet. Chem.*, 2011, **696**, 255–262.
27 H.-L. Teng, Y. Luo, M. Nishiura and Z. Hou, *J. Am. Chem. Soc.*, 2017, **139**, 16506–16509.
28 H.-L. Teng, Y. Luo, B. Wang, L. Zhang, M. Nishiura and Z. Hou, *Angew. Chem., Int. Ed.*, 2016, **55**, 15406–15410.
29 A. A. Trifonov, I. V. Basalov and A. A. Kissel, *Dalton Trans.*, 2016, **45**, 19172–19193.
30 B.-T. Guan and Z. Hou, *J. Am. Chem. Soc.*, 2011, **133**, 18086–18089.
31 J. Oyamada and Z. Hou, *Angew. Chem., Int. Ed.*, 2012, **51**, 12828–12832.
32 B.-T. Guan, B. Wang, M. Nishiura and Z. Hou, *Angew. Chem., Int. Ed.*, 2013, **52**, 4418–4421.
33 G. Song, W. W. N. O[illegible]d Z. Hou, *J. Am. Chem. Soc.*, 2014, **136**, 12209–12212.
34 X. Shi, M. Nishiura and Z. Hou, *J. Am. Chem. Soc.*, 2016, **138**, 6147–6150.
35 Y. Luo, H.-L. Teng, M. Nishiura and Z. Hou, *Angew. Chem., Int. Ed.*, 2017, **56**, 9207–9210.
36 S. Arndt and J. Okuda, *Adv. Synth. Catal.*, 2005, **347**, 339–354.
37 P. M. Zeimentz, S. Arndt, B. R. Elvidge and J. Okuda, *Chem. Rev.*, 2006, **106**, 2404–2433.
38 S. Arndt and J. Okuda, *Chem. Rev.*, 2002, **102**, 1953–1976.
39 A. A. Trifonov, in *Olefin Upgrading Catalysis by Nitrogen-based Metal Complexes*, ed. C. J. a. G. G., Springer, Dordrecht, 2011, vol. 34, pp. 119–152.
40 Z. Hou, Y. Luo and X. Li, *J. Organomet. Chem.*, 2006, **691**, 3114–3121.
41 M. Zimmermann, K. W. Törnroos and R. Anwander, *Angew. Chem., Int. Ed.*, 2008, **47**, 775–778.
42 D. Li, S. Li, D. Cui and X. Zhang, *Organometallics*, 2010, **29**, 2186–2193.
43 K. Lv and D. Cui, *Organometallics*, 2010, **29**, 2987–2993.
44 L. Wang, D. Cui, Z. Hou, W. Li and Y. Li, *Organometallics*, 2011, **30**, 760–767.
45 Y. Luo, S. Fan, J. Yang, J. Fang and P. Xu, *Dalton Trans.*, 2011, **40**, 3053–3059.
46 D. Robert, E. Abinet, T. P. Spaniol and J. Okuda, *Chem. – Eur. J.*, 2009, **15**, 11937–11947.
47 G. Du, Y. Wei, L. Ai, Y. Chen, Q. Xu, X. Liu, S. Zhang, Z. Hou and X. Li, *Organometallics*, 2011, **30**, 160–170.
48 S. Li, D. Cui, D. Li and Z. Hou, *Organometallics*, 2009, **28**, 4814–4822.
49 L. Li, C. Wu, D. Liu, S. Li and D. Cui, *Organometallics*, 2013, **32**, 3203–3209.
50 Y. Pan, T. Xu, G.-W. Yang, K. Jin and X.-B. Lu, *Inorg. Chem.*, 2013, **52**, 2802–2808.
51 W. Rong, D. Liu, H. Zuo, Y. Pan, Z. Jian, S. Li and D. Cui, *Organometallics*, 2013, **32**, 1166–1175.
52 L. Wang, D. Liu and D. Cui, *Organometallics*, 2012, **31**, 6014–6021.
53 X. Li and Z. Hou, *Coord. Chem. Rev.*, 2008, **252**, 1842–1869.
54 M. Nishiura and Z. Hou, *Nat. Chem.*, 2010, **2**, 257.
55 M. Zimmermann, O. Nuyken and W. Obrecht, in *Advances in Polymer Science*, ed. O. Nuyken, Springer-Verlag, Berlin, Heidelberg, 2006.
56 L. S. Baugh and J. A. M. Canich, *Stereoselective Polymerization with Single-Site Catalysts*, CRC Press/Taylor & Francis, New York, 2008.
57 Z. Zhang, D. Cui, B. Wang, B. Liu and Y. Yang, in *Molecular Catalysis of Rare-Earth Elements*, ed. P. W. Roesky, Springer Berlin Heidelberg, Berlin, Heidelberg, 2010, pp. 49–108, DOI: 10.1007/430_2010_16.
58 D. Takeuchi, in *Encyclopedia Of Polymer Science and Technology*, John Wiley & Sons, 2013, DOI: 10.1002/0471440264.pst595.
59 H. Wang, Y. Zhao, M. Nishiura, Y. Yang, G. Luo, Y. Luo and Z. Hou, *J. Am. Chem. Soc.*, 2019, **141**, 12624–12633.
60 H. Wang, Y. Yang, M. Nishiura, Y. Higaki, A. Takahara and Z. Hou, *J. Am. Chem. Soc.*, 2019, **141**, 3249–3257.
61 C. Wang, G. Luo, M. Nishiura, G. Song, A. Yamamoto, Y. Luo and Z. Hou, *Sci. Adv.*, 2017, **3**, e1701011.
62 S. Li, D. Liu, Z. Wang and D. Cui, *ACS Catal.*, 2018, **8**, 6086–6093.
63 B. Liu, S. Li, M. Wang and D. Cui, *Angew. Chem., Int. Ed.*, 2017, **56**, 4560–4564.
64 Z. Hou and Y. Wakatsuki, *Coord. Chem. Rev.*, 2002, **231**, 1–22.
65 L. Zhang, T. Suzuki, Y. Luo, M. Nishiura and Z. Hou, *Angew. Chem., Int. Ed.*, 2007, **46**, 1909–1913.
66 W. Gao and D. Cui, *J. Am. Chem. Soc.*, 2008, **130**, 4984–4991.
67 L. Zhang, M. Nishiura, M. Yuki, Y. Luo and Z. Hou, *Angew. Chem., Int. Ed.*, 2008, **47**, 2642–2645.
68 Y. Yang, K. Lu, L. Wang, Y. Wang and D. Cui, *Chem. Commun.*, 2010, **46**, 6150–6152.
69 B. Wang, D. Cui and K. Lv, *Macromolecules*, 2008, **41**, 1983–1988.
70 H. Liu, J. He, Z. Liu, Z. Lin, G. Du, S. Zhang and X. Li, *Macromolecules*, 2013, **46**, 3257–3265.

71 C. Yao, D. Liu, P. Li, C. Wu, S. Li, B. Liu and D. Cui, *Organometallics*, 2014, **33**, 684–691.
72 T. Matsuo and H. Kawaguchi, *J. Am. Chem. Soc.*, 2006, **128**, 12362–12363.
73 S. J. Mitton and L. Turculet, *Chem. – Eur. J.*, 2012, **18**, 15258–15262.
74 Y. Jiang, O. Blacque, T. Fox and H. Berke, *J. Am. Chem. Soc.*, 2013, **135**, 7751–7760.
75 P. Rios, A. Rodriguez and J. Ljpez-Serrano, *ACS Catal.*, 2016, 5715–5723.
76 A. Berkerfeld, W. E. Piers, M. Parvez, L. Castro, L. Maron and O. Eisenstein, *Chem. Sci.*, 2013, **4**, 2152–2162.
77 F. A. LeBlanc, W. E. Piers and M. Parvez, *Angew. Chem., Int. Ed.*, 2014, **53**, 789–792.
78 L. Luconi, A. Rossin, G. Tuci, Z. Gafurov, D. M. Lyubov, A. A. Trifonov, S. Cicchi, H. Ba, C. Pham-Huu, D. Yakhvarov and G. Giambastiani, *ChemCatChem*, 2019, **11**, 495–510.
79 D. M. Lyubov, L. Luconi, A. Rossin, G. Tuci, A. V. Cherkasov, G. K. Fukin, G. Giambastiani and A. A. Trifonov, *Chem. – Eur. J.*, 2014, **20**, 3487–3499.
80 C. Gorton and E. Eugene, in *Bond Energies*, ed. C. Gorton, Tennessee, Southwestern, 2002, vol. 1.
81 A. W. Addison, T. N. Rao, J. Reedijk, J. van Rijn and G. C. Verschoor, *J. Chem. Soc., Dalton Trans.*, 1984, 1394–1356.
82 J. Blackwell, C. Lehr, Y. Sun, W. E. Piers, S. D. Pearce-Batchilder, M. J. Zaworotko and V. G. Young Jr., *Can. J. Chem.*, 1997, **75**, 702–711.
83 G. Du, Y. Wei, W. Zhang, Y. Dong, Z. Lin, H. He, S. Zhang and X. Li, *Dalton Trans.*, 2013, **42**, 1278–1286.
84 W. Gao, D. Cui, X. Liu, Y. Zhang and Y. Mu, *Organometallics*, 2008, **27**, 5889–5893.
85 E. Lu, J. Chu, Y. Chen, M. V. Borzov and G. Li, *Chem. Commun.*, 2011, **47**, 743–745.
86 P. Zhang, H. Liao, H. Wang, X. Li, F. Yang and S. Zhang, *Organometallics*, 2017, **36**, 2446–2451.
87 L. Luconi, D. M. Lyubov, A. Rossin, T. A. Glukhova, A. V. Cherkasov, G. Tuci, G. K. Fukin, A. A. Trifonov and G. Giambastiani, *Organometallics*, 2014, **33**, 7125–7134.
88 S. Bambirra, A. Meetsma and B. Hessen, *Organometallics*, 2006, **25**, 3486–3495.
89 D. J. Parks, J. M. Blackwell and W. E. Piers, *J. Org. Chem.*, 2000, **65**, 3090–3098.
90 D. J. Parks and W. E. Piers, *J. Am. Chem. Soc.*, 1996, **118**, 9440–9441.
91 V. Gevorgyan, M. Rubin, S. Benson, J.-X. Liu and Y. Yamamoto, *J. Org. Chem.*, 2000, **65**, 6179–6186.
92 S. Bontemps, *Coord. Chem. Rev.*, 2016, **308**, 117–130.
93 F. J. Fernández-Alvarez, A. M. Aitani and L. A. Oro, *Catal. Sci. Technol.*, 2014, **4**, 611–624.
94 M. Cokoja, C. Bruckmeier, B. Rieger, W. A. Herrmann and F. E. Kuhn, *Angew. Chem., Int. Ed.*, 2011, **50**, 8510–8537.
95 Upon treatment with $B(C_6H_5)_3$, $\mathbf{1_Y}^{\mathbf{THF}}$ behaved similarly. The cationization process though was slower at the beginning of the reaction, probably because of the more crowded metal coordination sphere.
96 M. F. Lappert and R. Pearce, *J. Chem. Soc., Chem. Commun.*, 1973, 126–126.
97 S. J. Lyle and M. M. Rahman, *Talanta*, 1963, **10**, 1177–1182.
98 *Bruker-AXS*, 2014.
99 G. M. Sheldrick, *Acta Crystallogr., Sect. C: Struct. Chem.*, 2015, **71**, 3–8.
100 L. Krause, R. Herbst-Irmer, G. M. Sheldrick and D. Stalke, *J. Appl. Crystallogr.*, 2015, **48**, 3–10.